EXPERIMENTAL MEASUREMENTS BY VARIOUS INSTRUMENTATIONS TO ANALYSE DATA FOR MODELLING DPM CONCENTRATIONS IN UNDERGROUND MINES

by

NURSULTAN MAGAUIYA

THESIS SUPERVISOR

PROFESSOR SERGEI SABANOV

Thesis submitted to the School of Mining and Geosciences of Nazarbayev University in Partial Fulfillment of the Requirements for the Degree of
Master of Science in Mining Engineering

Nazarbayev University
17 APRIL 2022

ORIGINALITY STATEMENT

I, Nursultan Magauiya, hereby declare that this submission is my own work and to the best of my knowledge it contains no materials previously published or written by another person, or substantial proportions of material which have been accepted for the award of any other degree or diploma at Nazarbayev University or any other educational institution, except where due acknowledgement is made in the thesis.

Any contribution made to the research by others, with whom I have worked at NU or elsewhere is explicitly acknowledged in the thesis.

I also declare that the intellectual content of this thesis is the product of my own work, except to the extent that assistance from others in the project's design and conception or in style, presentation and linguistic expression is acknowledged.

Signed on 13 APRIL 2022

ABSTRACT

During underground mining operations, the ventilation system provides fresh air to reduce the impact of diesel engine exhaust gasses. Most dangerously, diesel particulate matter (DPM), is known to be a cancer - causing factor when inhaled for a sustained length of time in these diesel-powered vehicles. This problem is widespread in the mining industry, also in Kazakhstan. Diagnostic and monitoring technologies for DPM in the mining sector are still in their development stage, as well as approaches for detecting DPM in underground mines. The main objective of this thesis is to conduct experimental measurements by various instrumentations to analyze data for modelling DPM concentrations in underground mines. In order to achieve this goal, the existing literature is reviewed, and the methodology from these studies was modified in accordance with the measurements, that were done in the underground mine of Eastern Kazakhstan region. From the measurements, the data of airflow velocity, particulate matters, black carbon concentration, lung deposited surface area concentration, and particle diameters were obtained. The measuring instruments are anemometer, RizgardPM, Microaeth, and Partector. From these instruments the velocity, different Particulate Matter (PM1, PM2.5, and PM10), black carbon concentration, and lung-disposal surface area values were received, accordingly. The results from these tools were analyzed based on correlation factors. The ANSYS CFD software were used to simulate the velocity for this thesis. Initially, the data was analyzed for modeling purposes and were taken using equipment from underground measurements. In addition, the geometry of the mine was created in accordance with mine surveyor data and laser measurements directly from the underground mine. As a result, the preliminary velocity simulation is done.

DEDICATION

I would like to thank my professor, Dr. Sergei Sabanov for his irreplaceable contribution, patience, support, and motivation for this thesis.

I would like to thank faculty Dean, Professors, Associate Professors, all managers, and laboratory assistants for allowing me to be a part of this master's study.

I would like to thank PhD candidate Abdullah Rasheed Qureshi for his assistance in technical regulations of my thesis.

I would like to thank my classmates for assisting in some questions during studies.

I would like to thank my friends, Islam I, Iliya Victorovich Z, Adilet M, and Daniyar T for steering me in the right direction.

I would like to thank my younger sister and brother, Inzhu and Nurislam for motivating me to be the best version of myself.

I would like to thank my parents, both grandmothers, and grandfather for accepting me for who I am.

Wholeheartedly, I am so sorry for the loss of family members during the Russian-Ukrainian conflict in 2022. I want both states to find a common language at the negotiating table.

In loving memory of Professor Laurent Richard, who asked for so little but gave so very much.

ACKNOWLEDGMENT

This study was supported by Nazarbayev University Grant Programs: **Research Grant #090118FD5337** and **Collaborative Research Project # 091019CRP2104.**

TABLE OF CONTENT

LIST OF FIGURES

LIST OF TABLES

1. INTRODUCTION

1.1 Background

Mining equipment powered by diesel fuel is extensively employed in underground mines. Diesel engines are an appealing choice in the mining sector not only because they can convert the majority of available energy into meaningful labor, but also because they are cost-effective, reliable, and stable. Diesel equipment in underground mines often offers more flexibility and mobility in comparison to electric systems (Khan, 2017). Compared to equipment powered by on-board battery-powered devices, diesel equipment provides more power and higher operational readiness, since it eliminates the need for a long battery replacement, as well as more time to recharge the battery (Nieto, Schatz, and Dogruoz, 2020).

On the downside, the usage of diesel equipment has a detrimental effect on underground miners. The many poisonous gasses emitted by machinery, such as carbon monoxide, carbon dioxide, nitrogen oxide, nitrogen dioxide, sulfur dioxide, aldehydes, and others, offer substantial health risks to the miners who are exposed to this kind of mine environment. Diesel particulate matter (DPM) is the most dangerous component of diesel exhaust gases, and they are present in high concentrations because it depends on the efficiency of the ventilation system. When compared to other sectors, the risk of miners being overexposed to DPM and other toxic gasses is higher in underground mines because of the tight conditions (Sagesh Kumar, Dash, Bhattcharjee, and Panigrahi, 2018).

1.2 Problem Definition

Diagnostic and monitoring technologies for DPM in the mining sector are still in their development stage, as well as approaches for detecting DPM in underground mines. Compliance with these rules was not difficult for the coal mining industry. U.S. Mine Safety and Health Administration (MSHA) officials, on the other hand, have claimed that many underground metal and non-metal mines are still experiencing difficulties achieving the regulation limit (Zheng, 2011).

Diesel particulate matter is a sub-micron aerosol produced by incomplete combustion of fuel and lubricant hydrocarbons. In addition to engine design and life, exhaust after treatment devices and equipment operators all affect the composition of diesel exhaust (Khan, 2017). In fact, 90% of DPM is below 0.1 μm in size. Due to its small size, it will remain in the air for an

extended period of time, polluting the underground mining environment and posing health risks to miners. This can lead to things such as cancer or asthma (Thiruvengadam, Zheng, and Tien, 2016). There are some techniques to control DPM in the mine developed by NIOSH, which can monitor elemental carbon in relation to DPM. But, there are no techniques to measure and monitor exactly DPM concentrations directly.

1.3 Objectives of the Thesis

1.3.1 Main Objective

The main aim of this thesis is to conduct experimental measurements by various instrumentations to analyze data for modelling DPM concentrations in underground mines.

1.3.2 Specific Objectives

- Make a comprehensive literature review on DPM emissions measurements in underground mines, mine ventilation CFD modeling, DPM control strategies
- Conduct experimental measurements by various instrumentations in underground mine conditions
- Analyse received data from the experimental measurements
- Evaluate suitability of the used instrumentations for DPM sampling and monitoring
- Validate the received data for CFD modelling of auxiliary ventilation in underground mines

1.4 Hypotheses

To establish DPM sampling and monitoring strategies for Kazakhstani metal mines, monitoring elemental carbon (EC) and total carbon (TC) can be proposed. The monitoring will be done continuously using RizgardPM tool monitors for PM1. As a result, it would be possible to define the EC. Moreover, the source of elemental carbon is smoking cigarettes, thus during the measurements it should be considered. For continuous measurements, using another tool – Microaeth, the black carbon concentration would be defined simultaneously in active ore heading zones. The PM1 and BC are surrogate for DPM. EC and BC can be harmonized to find a calibration factor to correct continuous BC measurements and obtain continuous EC

concentrations. Once EC is obtained, the EC can be deducted from TC to obtain real-time OC concentrations. From PM1 and BC sampling the DPM concentrations could be derived, and used for monitoring.

1.5 Justification of the R&D

Kazakhstan has a large number of mines that generate dangerous pollutants. One of these pollutants is diesel exhaust gases and particulate matter (PM). Several new mines are being built underground as Kazakhstan's mining sector expands. In order to keep miners safe, the ventilation system in the mine must provide them with clean air. Because the well-being of those working in the mine is of the greatest priority. The majority of miners in Kazakhstan are exposed to DPM and other fumes from diesel engine equipment that is still in operation. New technologies and ways to decrease emissions are constantly being developed because of stricter emission limits. Miners' exposure to diesel emissions may be reduced by developing techniques to manage diesel pollutants. Design of an underground mine ventilation system must adhere to health and safety regulations. The mining sector will benefit from this research by improving local rules for regulating pollutant and dust dilution. This research will assess the present state of affairs in the mines of Eastern Kazakhstan. With this information, an underground mine's auxiliary ventilation can be optimized to reduce DPM concentrations in the area of active ore heading. In the future, the optimization of financial expanses could be done. These achievement needs calculations by using Ventsim software.

1.6 Scope of Work

Scope of work is based on the proposed objectives and will include following:

1. Introduction defines problem statement and the study's objectives, hypotheses, scope of work, and significance to the mining industry.
2. Literature review summarizes the existing DPM measurements and controlling strategies.
3. Research methodology describes the study´s limitations, data acquisition, and approaches to sampling, measurements, test works, modelling and data analysis.
4. Results presence experimental test works and data analysis.
5. Conclusions and recommendations summarize the main results of the analysis and provide recommendations for further studies.

2. LITERATURE REVIEW

2.1 Diesel Particulate Matter

Due to the combination of solid and liquid particles that diesel engines emit into the atmosphere, diesel engines are a significant source of pollution in terms of particulate matter (PM) emissions (Ristovski, Miljevic, Surawski, Morawska, Fong, Goh, Yang, 2012). Concentrated diesel particles get denser as their particle size rises (Zheng 2011, as cited in Morla and Karekal, 2017). In diesel exhaust, the composition of the gaseous and particulate matter changes depending on the environmental conditions in which the engines are operating (Khan, 2017).

Diesel particulate matter is made of a large number of extremely tiny particles (nanometers) with very little amount of material mixed together with a few larger particles (micrometers) that make up the majority of the overall mass (as seen in Figure 1). The particle sizes are classified as follows (Morla and Karekal, 2017):

- Nano particles size: less than 50 nm;
- Ultra-fine particle size: less than 100 nm;
- Fine particle size: less than 2.5 μm;

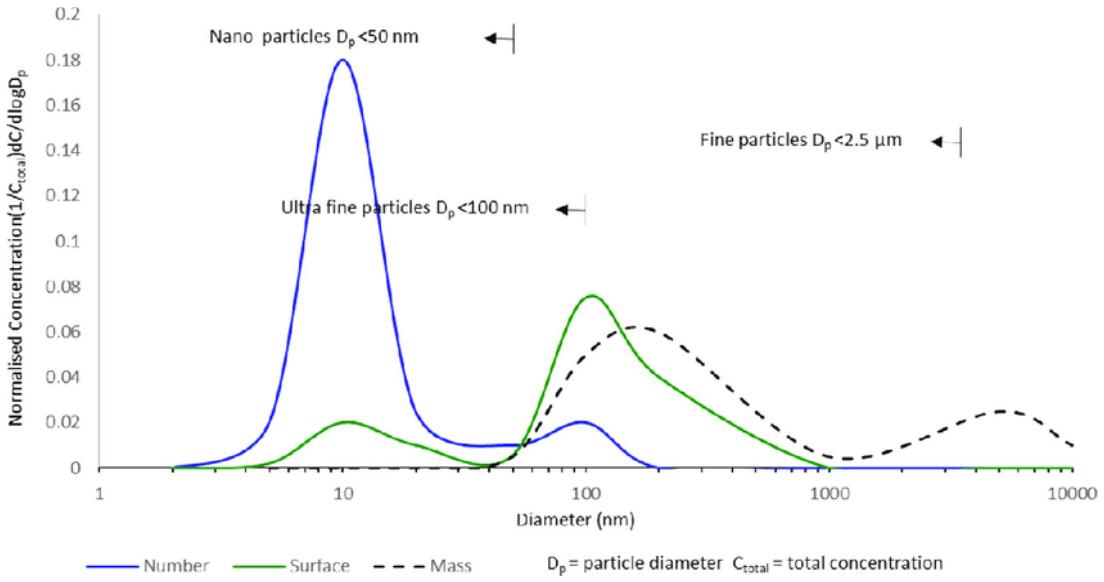

Figure 1. DPM size distribution: by number, surface area, and mass. Source: Morla and Karekal, 2017.

Medical experts believe that if people are exposed to diesel exhaust for an extended length of time, it has the potential to cause cancer. Asthma, inflammation of the eyes and nose,

headaches, and nausea have all been related to short-term exposure to diesel fumes, according to research (Levin and Semin, 2017). As a result, addressing diesel particulate matter management is crucial.

2.2 Diesel Particulate Matter Control Strategies

Diesel engines utilized in underground mines have a severe influence on miners because of the toxic exhaust gasses and particle components like DPM that they produce (Stanek and Brown, 2019).

Carbon and organic polymer waste comprise the vast bulk of submicrometer particles. Fine particles, on the other hand, account for 78% to 98% of carbonaceous material. The mining and blasting sector have long used black carbon as a tracer for diesel emissions (Noll, Bugarski, Patts, Mischler, and McWilliams, 2007; Noll, and Janisko, 2013, as cited in Saarikoski, Salo, Bloss, Alanen, Teinila, Reyes, ... and Timonen, 2019). During underground mining, diesel engines are responsible for producing somewhere between 35% and 84% of the PM1 pollution (Saarikoski et al. 2019).

According to Choi, Park, Kim, Kim, Lee, Chung, ... and Park (2020), black carbon is an "excellent" indication of exposure to diesel exhaust. The burning of biomass, biofuels, and fossil fuel combustion products, among other things, produces black carbon as a byproduct. Vehicles powered by diesel engines produce much higher levels of fine particulate matter than those powered by gasoline engines. The problem with black carbon is exacerbated by inadequate ventilation in the underground.

The largest concentrations of CO_2 emissions are seen during ore transportation using dump trucks and conveyor belts, with average concentrations ranging between 950-1440 parts per billion. In addition, NO_x emissions ranged from 960 to 1900 ppb during ore transportation (Robinson, Olson, Liu, and Schauer, 2015, as cited in Saarikoski et al. 2019). These values could be reduced after efficient ventilation.

When used in combination with other pollution control products, diesel particulate filters (DPF) can significantly reduce soot emissions from vehicles (Robinson, Olson, Liu, and Schauer, 2015, as cited in (Saarikoski et al. 2019). The advantage of this filter type is underlined by Choi, Park, Kim, Kim, Lee, Chung, ... and Park (2020), where the authors stated that DPF technology placed on diesel-powered vehicles greatly decreases the quantity of black carbon

emitted by these engines. Recirculation of exhaust gases decreases pollution by reducing NOx emissions; however, it may potentially increase PM emissions (Saarikoski et al. 2019).

In the combustion process, elemental carbon (EC) emissions are part of the DPM. Diesel engine characteristics influence the consistency of EC, and DPM accounts for about 80% of the overall quantity of EC in the atmosphere (Choi et al., 2020).

Total carbon (TC) is represented at 80 percent in DPM, which is similar to the representation of elemental carbon. Figure 2a show the results of a regression study examining the association between TC) and elemental carbon content. If diesel particulate filters are not installed, it is possible to anticipate the amount of diesel particulate matter in an isolated region using parts per million and EC. As shown in Figure 2b, when uncatalyzed DPF was used in isolated zone tests, a connection was established between DPM and EC (Noll, Bugarski, Patts, Mischler, and McWilliams, 2007).

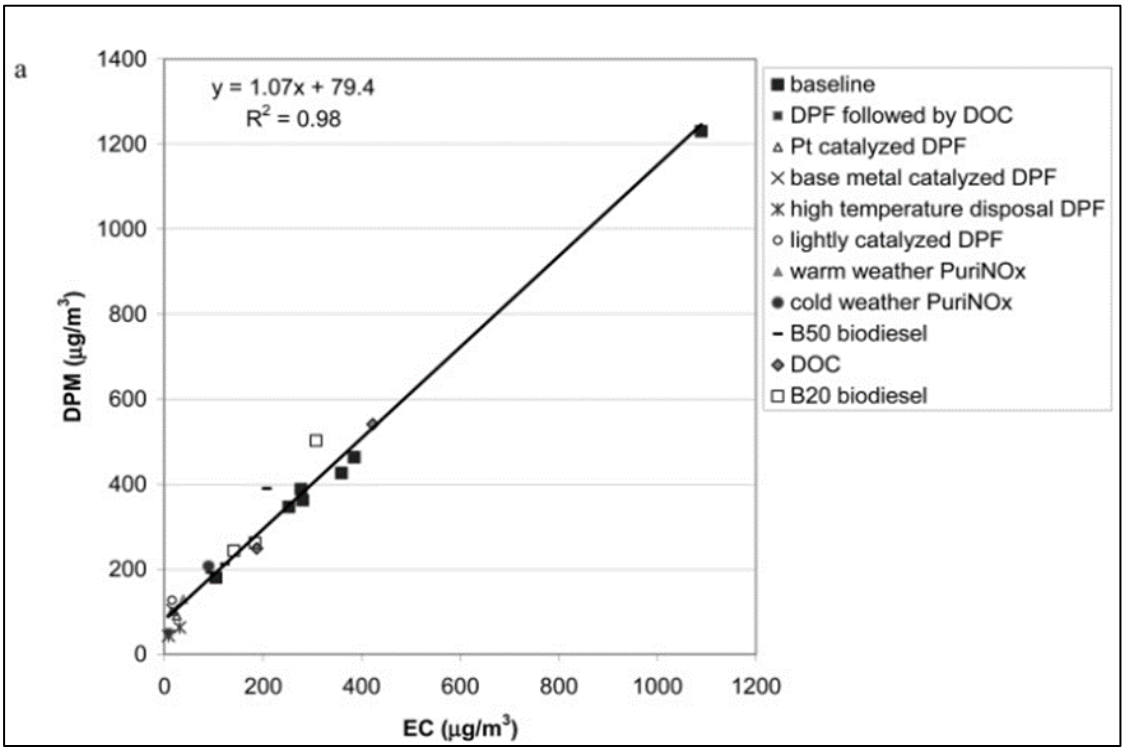

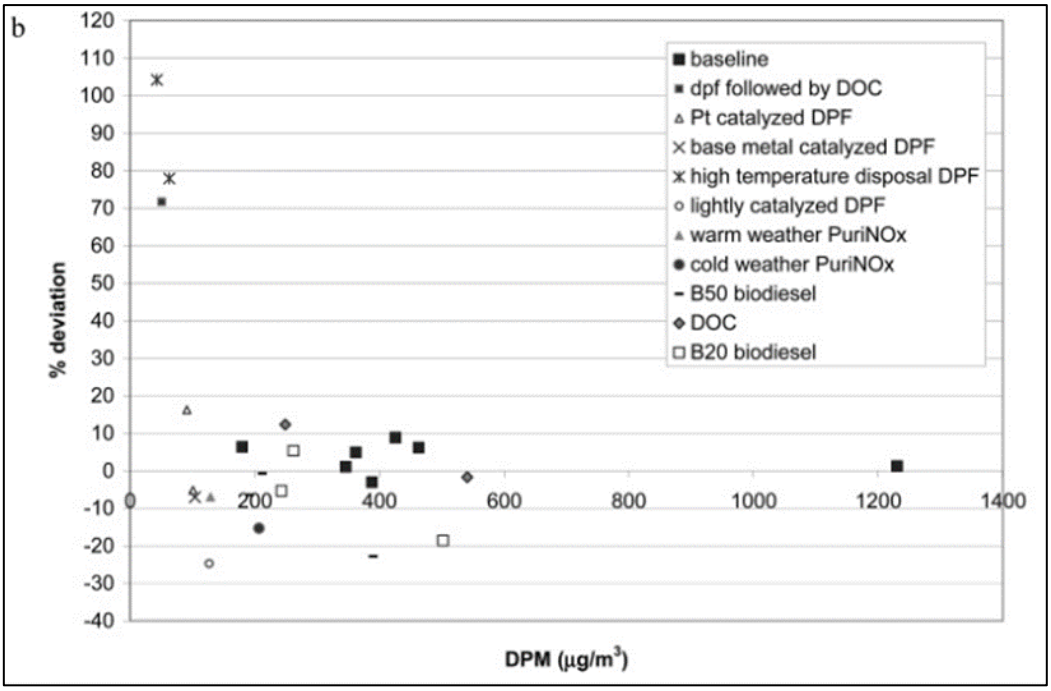

Figure 2 (a) linear regression chart for DPM vs EC for data from vehicles in the isolated zone study. (b) Percent deviation of the measured DPM values from the calculated DPM from EC using the equation of the line. Source: Noll, Bugarski, Patts, Mischler, and McWilliams, 2007.

According to Figure 2a, DPM and EC correlate by almost 98%. If DPFS are utilized in underground mines, it will be able to reduce the amount of DPM produced. Given that the EC accounts for more than 80 percent of DPM, this connection provides an indication of how elemental carbon will interact with DPM over time (Noll, Bugarski, Patts, Mischler, and McWilliams, 2007).

2.3 Existing Methods of Reducing DPM at the Engine Exhaust

DPM emissions may be regulated in addition to the use of DPF filters by mitigation and preventative measures (Stephenson, Lutte, and Spear, 2006) as well as source and exposure as controlling methods (Chang and Pu, 2019). According to Stephenson, Lutte and Spear (2006), the purpose of mitigation approaches is to minimize and eliminate DPM from the environment before it is discharged into the atmosphere. That might be accomplished via the use of the best diesel engines, DPF filters, and alternate fuels (biodiesel reduces DPM emissions by 47%) (Chang and Pu, 2019), and sophisticated maintenance methods. If DPM has been discharged, further controls such as mine ventilation, closed cabins with filtered breathing air equipment, and administrative controls must be considered. According to Chang and Pu (2019), pre-discharge source control is a method for limiting diesel particulate matter emissions from diesel

engines. In case, if DPM emissions are already released exposure controls are used. DPF filters, effective ventilation, and post-treatment protective devices may all be used to achieve exposure management. Mcginn (2000) confirms maintenance as a reduction factor of DPM in findings. Bugarski, Cauda, Janisko, Mischler, and Noll (2011) revealed the importance of diesel engine maintenance (as cited in Chang and Pu, 2019). According to Bugarski, Cauda, Janisko, Mischler, and Noll (2011), "maintaining the efficiency of the engine compression system, cooling systems" are the proposed maintenance methods for mining companies. As a result, an external exhaust gas recirculation system will be monitored. Additionally, operators and engineers may begin by frequently inspecting and repairing their diesel engines to decrease DPM emissions, since this is a very inexpensive and simple task (Chang and Pu, 2019).

There have been a number of studies showing that diesel particulate emissions may be effectively decreased by using filters (three-dimensional simulation study by Yang, Deng, Gao, and He (2016); Haney, Fields, and Vail (1997); and Chang and Pu (2019). In accordance with Haney, Fields, and Vail (1997), while diesel particulate filters have a removal effectiveness of 60% to 90%, the use of diesel oxidation catalysts may reduce diesel particulate matter emissions by up to 50%. These filters have the greatest efficiency when using the engine at full power, which leads to a reduction in mass concentration of up to 40 percent.

Another method of monitoring DPM, approved by the Mine Safety and Health Administration, is to collect air samples. DustTrak tool could be used for that purpose with the cut-off point for sampling being 0.9 μm (Stephenson, Lutte, and Spear, 2006).

Stephenson et al. 2006 used DustTrak data with a one-minute interval to determine the average particle mass concentration during the sampling session. Sample data were analyzed using regression to see whether there was a connection between where the impact components were and where the monitor was. To determine the relationship between exposure-induced TC concentrations and average mass concentrations along the dust route, researchers used a regression analysis (Table 1. DPM Samples Results. Source: Stephenson, Lutte, and Spear, 2006.). The correlation (determination coefficient $R^2 = 0.91$) between the findings of the SKC® impactor concentration measurement and the DustTrak concentration measurement is high (Figure 3) (Stephenson, Lutte, and Spear, 2006).

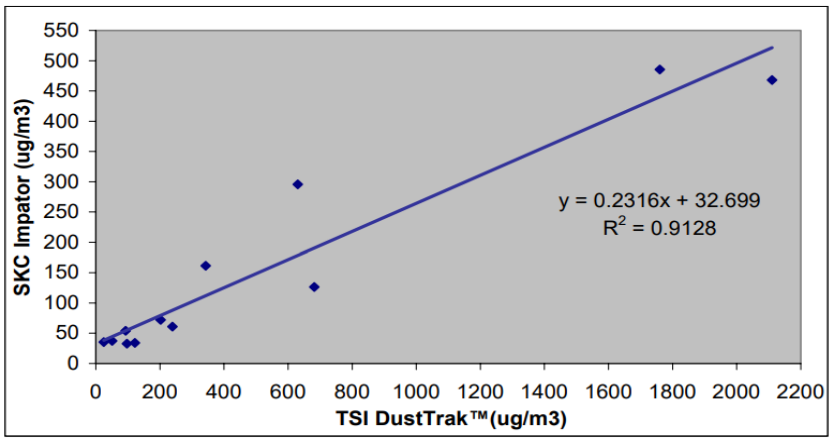

Figure 3. Correlation between TSI® DustTrak™ and SKC® Impactor. Source: Stephenson, Lutte, and Spear, 2006.

Table 1. DPM Samples Results. Source: Stephenson, Lutte, and Spear, 2006.

Date	Mine location	OC, $\mu g/cm^3$	EC, $\mu g/cm^3$	TC, $\mu g/cm^3$	DustTrak™, $\mu g/cm^3$
1/14/00	Mine Shaft	<17	<17	<34	120
1/14/03	Ore Face	98	370	470	2100
1/14/03	Mine Shop	<19	<19	<37	51
1/15/03	Mine Shaft	<19	<18	<36	25
1/15/03	Ore Face	130	350	490	1800
1/15/03	Mine Shop	<19	36	<54	93
1/16/03	Ore Dump	<16	<16	<32	97
1/16/03	Ore Face	48	78	130	680
1/16/03	Mine Shop	<20	41	<61	240
1/17/03	Ore Face	51	110	160	340
1/17/03	Ore Face	84	210	300	630
1/17/03	Mine Shop	30	42	72	200

From the findings by Stephenson, Lutte, and Spear (2006), the correlation between the SKC® impactor and the TSI® DustTrak particle sensor may be used to determine the magnitude of time-integrated DPM concentrations.

There are some techniques to control DPM in the mine developed by NIOSH:

- Elemental carbon optical monitor (correlation R^2=0.998 between EC and DPM) by Noll and Janisko (2007);
- ICx DPM Monitor beta prototype by Janisko and Noll (2010);
- Airtel ICx DPM monitor by Noll and Janisko (2013);
- Grimm Model 1.109 Real-Time Aerosol Monitors by Kimbal, Pahler, Larson, VanDerslice (2012);
- AE33 Aethalometer, Airwatch and The Semi-Continuous OC-EC Field Analyzer by Barrett, Sarver, Cauda, Noll, Vanderslice, and Volkwein (2019).

Instantaneous evaluation of on-board DPM enables rapid application of control measures, safeguarding the health of impacted miners (Stephenson, Lutte, and Spear, 2006). Because of these findings the mining industry is able to evaluate the direct human effect of DPM as it occurs.

2.4 Ventilation for DPM Dilution

A ventilation system is an example of an engineering control. Reduced exposure to DPM, exhaust gases, and heat in underground mines is made possible by the installation of ventilation systems. The most frequent and most successful technique of reducing DPM is ventilation dilution, even if other approaches exist. Ventilation may be improved by increasing airflow, either by utilizing fans that are more powerful or by adding more fans in conjunction with existing ones in mines with mechanical ventilation. To further reduce their energy use, they may swap out their existing fan engine with a less powerful, more efficient one (Brake, 2013). Chang, Xu, Zhou, Mullins, Abishek (2019), support these advantages in study where the authors stated that ventilation is still the most often used strategy. The use of a ventilation duct for auxiliary ventilation in an underground mine development face is common since it is less expensive. As a result, a cost-effective and efficient design for the secondary air ducts is required (with the shortest possible duct length). Moreover, the authors Torano, Torno, Menendez, and Gent, 2011 stated that with the use of dust control technology, the quality of the auxiliary ventilation system is critical in ensuring a safe working environment for those who work underground.

For ventilation, propeller fans are superior to blade-axial fans because they provide greater airflow at lower static pressures. Fans with fewer blades and superior aerodynamics should be used. The National Institute for Occupational Safety and Health (NIOSH) has created ventilation concepts for major mines. Separated shaft structures and ventilation-based structures are two examples. The perimeter of the mine is better ventilated thanks to the installation of an air wall between the active mining areas and the remainder of the mine. Natural ventilation and extra fans may frequently be used in conjunction with natural ventilation to ventilate the enormous storage chambers found in many major mines (Bugarski, Janisko, Cauda, Mischler, and Noll, 2012).

Auxiliary ventilation is used in all mines, metallic and non-metallic, to keep the air in the working areas fresh. In the same way that perimeter ventilation utilizes air barriers to steer air, downhole ventilation of a mine employs this method. For advanced mines, separate shaft

ventilation, such as block ventilation, is ideal. Return airshafts expanding with funnels and existing mines benefit greatly from this method. Supplying fresh air at distances of 30 meters or more may be accomplished using a fan and piped system (Bugarski, Janisko, Cauda, Mischler, and Noll, 2012).

It is the most recent advancement in ventilation monitoring and management: ventilation on-demand (VOD) and cooling on-demand (COD). Both of these techniques must be used in conjunction with one another in order to guide and manage the amount and quality of air. Using the VOD technique might save money on ventilation costs since greater air would be delivered if diesel machinery is running. Another benefit of the VOD technique is that the control of diesel fumes, DPM, and dust will be more effective. From the findings by Gyamfi (2020), the VOD system was considered in different scenarios. And these scenarios include the amount of operating equipment. As a result, the VOD could be used during the DPM dilution. The most effective strategy to keep expenses under control is to use a variety of strategies. Instead than resisting DPM, it was intended for improving air quality in tunnels (Bugarski, Janisko, Cauda, Mischler, and Noll, 2012).

A recent study by Chang, Xu, Zhou, Mullins, Abishek (2019) in Western Australia analyzed a physical model of an underground mine inside the limits of a mine face and utilized computational fluid dynamics to investigate the concentration of DPM and airflow within the mine face. It was found that DPM concentrations were not reduced by the present ventilation system, but the ventilation system with a reduced duct length of 5 meters was shown to be more successful in reducing DPM concentrations than the current ventilation system.

2.5 Computational Fluid Dynamics Modelling DMP Emissions

Computational fluid dynamics as one of the modeling techniques can be used to maintain existing ventilation systems, help improve control strategies, and identify high DPM concentrations. There are many studies done for the mining industry using this method. According to the authors (Zheng, Thiruvengadam, Lan, and Tien, 2015), the simulation findings may be used to develop effective working methods and to choose DPM reduction technology. DPM modeling makes use of both continuous and discrete phases to ensure that it is as accurate as feasible. Due to the critical nature of understanding the DPM dispersion scheme, CFD can assist in building a suitable ventilation system for the work area and connected entrances. Additionally, CFDs may be used to assess if additional control measures, such as ventilation, an environmental cabinet, or administrative control, are required to meet

regulatory standards. Numerous elements influence the dispersion of DPM, but the most critical are the kind of face, ventilation, diesel emissions, buoyancy impact, and direction of exhaust gas flow. The following studies use the Euler-Euler model, the Navier-Stokes equation, and the Lagrange technique to track particles. Authors to evaluate various simulation models use the ANSYS FLUENT environment.

Zheng, Thiruvengadam, Lan, and Tien (2015) claim that DPM was treated as a gas (continuous phase) and that n-octane vapor (C_8H_{18}) was used to simulate DPM in ANSYS software. The use of ANSYS software is justified due to its ability to produce the CFD simulations. And the equations for the steady state Navier–Stokes, continuity, and energy have been solved, and turbulence has been modeled using the traditional K-Epsilon turbulence model. It is feasible to include the buoyancy effect into the simulation by using gravity acceleration that is programmed to function vertically downwards (inlet flow, outlet flow, emissions source, and walls). Only a portion of the sweep surface was subjected to significant DPM exposure dangers because DPM is not evenly distributed over the exhaust cross-sectional plane. Therefore, the Navier-Stokes equation effectively regulates both the gas and particle phases. Moreover, the simulation findings may be used to build effective working approaches and to pick DPM reduction technology (Zheng et al., 2015). One year later, these authors, Thiruvengadam, Zheng and Tien (2016) examined the ANSYS simulation program to answer the question, whether or not the DPM will be considered a discrete or continuous (gas) when it reaches the isolated zone (particle). The critical setting is to use a Species Movement Model that incorporates DPM and ambient air. The diffusivity of air and DPM was determined based on their mixing properties. The temperature difference between the exhaust pipe and the fresh air intake caused substantial buoyancy, according to the computer model. As a result, DPM was dispersed unevenly throughout the single entry and concentrated toward the ceiling. The simulation demonstrated that both species transport and particle tracking models might be used to predict DPM dispersion patterns. Thiruvengadam et al. 2016 employed both transport and particle tracking models and were able to locate regions with elevated DPM concentrations in the critical zone around LHD sites.

Due to the discontinuous nature of DPM, it necessitates the use of Lagrangian particle tracking. To guarantee the accuracy of computations, high-density meshes are employed around the channel, wall, and LHD. By using grid independence analysis, it is feasible to strike the optimal balance between solution accuracy and computing costs. The Euler-Lagrange approach, as a discrete phase model, may provide more accurate findings in a shorter time span

than the Lagrangian method. Researchers may utilize the findings of various modeling techniques to deduce why DPM acts in such a unique way (Chang, Xu, Zhou, Mullins, Abishek, 2019). This research on the isolated entry was done at Noranda Inc.'s Brunswick mine and served as the foundation. At the basis of this investigation were three LHDs and three cargo transport vehicles. Four boundary conditions were included in the simulation: the main intake, the gaseous contaminant inlet, the walls of the underground opening, and the exhaust outlet for the diesel engine. In order to create a suitable CFD grid, all four CAD models were imported as systematic files from the CFD application and altered using GAMBIT.

In Chang et al. 2019, Eulerian-Eulerian method (EEM) and Eulerian-Lagrangian (ELM) particle tracking models were used to calculate and set the DPM emission rate at 2.49 10-6 kg/s. According to the Australian rules, equipment running on diesel fuel must have at least 0.06 m^3 of airflow. Study findings show favorable benefits from the ELM approach. In the end, researchers decided that DPM should be modeled by gaseous species (a species transfer phase model) with a lower diffusion coefficient. When developing a CFD model for any simulation, it is important to consider future computations, including the "shape" of a gas. Calibration of the simulated species' parameters may increase the simulation's accuracy (such as the diffusion coefficient and the mass flow rate at the inlet). As part of the discrete phase, the authors used the Lagrangian technique to monitor the DPM. Additional ventilation was added to the mine development face throughout the simulation. Because of the simulation, more effective supplementary ventilation solutions to the issue of growing DPM concentration may be offered (Chang et al., 2019).

2.5.1 CFD Simulation

By using CFD, it is possible to evaluate an air condition, as well as gas concentration during underground mining. Doctoral dissertation by Zheng (2011) provided information about existing studies about using CFD in mining industry:

- Heerden and Sullivan (1993) used CFD to assess the dust control for miners on a continual basis This study was able to calculate the airflow patterns using separate and distinctly mapped airflow velocity vectors over the entrance. Only trends in dust amounts were taken into consideration in order to determine how much dust was spread by the authors, who anticipated that dust particles would follow their own unique airflow velocity vector;

- Using a typical longwall face, Srinivasa, Baafi, Aziz, and Singh (1993) studied the effects of air velocity and dust control measures on the concentration of dust in the atmosphere.
- It was found that the nature of the airflow reflects the individual vector of the airflow velocity in the ventilation shafts of underground mines, and this was analyzed by Wala, Yingling, Zhang and Ray (1997). These patterns were shown to be true by looking at pressure and velocity data.
- Research has shown that computational fluid dynamics (CFD) can anticipate air pollution concentrations in indoor occupational situations. Although this study is not directly related to mining operations, it demonstrates the applicability of computational fluid dynamics (CFD) for gas and dust dispersion in underground mine entrances (Bennett, Crouch, and Shulman, 2003a; Bennett, Feigley, Khan, and Hosni, 2003b);
- Other researchers, Wala, Jacob, Huang, and Brown, 2003 investigated the effect of various cutting conditions on the flow structure in a continuous mine face. Further research by Wala, Vytla, Taylor, and Huang (2007), revealed that to maintain the same methane level in the face, about five times more air was required during the box cut than during the slab cut.
- With and without a continuous miner, Wala, Vytla, Huang, and Taylor (2008) looked at how methane was distributed on the surface. Also compared to experimental data, the simulation results were found to be largely consistent;
- At various main air stream speeds, Aminossadati and Hooman (2008) used a two-dimensional computational fluid dynamics (CFD) model to study the effects of brattice length on fluid flow behavior in the crosscut zones;
- CFD and experiments were utilized to investigate how airflow behaved at two-way junctions and splits by Jade and Sastry (2008). For some splits and junctions, the CFD shock loss coefficient and the results of an experiment in the flow domain were quite similar in terms of shock transfer. Shock loss coefficient findings ranged from 20% to 80%.
- Study by Zheng and Tien (2009) explored the distribution of methane on a longwall face. The CFD simulation demonstrated airflow patterns and high methane concentration zones when the shearer was installed in various locations. Methane dispersion was also studied in relation to walkway curtains, venturi water spray, and shearer drum airflow.

- In order to determine how much air was lost via the fan, Falk, Martin, and Keen (2010) employed computational fluid dynamics;
- Hurtado, Gutiérrez, and Moraga (2010) studied shock losses from block-caving production level deviations using computational fluid dynamics modeling. Simulated mine ventilation systems might be used to build more efficient ways in critical sites, according to the researchers;
- For the research, Purushotham and Bandopadhyay (2010) ran computer simulations of a variety of air-crossing configurations to see how shape affected shock losses. Within the scope of this research, it was hypothesized that CFD simulations would be able to accurately mimic the shock-loss phenomena associated with genuine air-crossing arrangements;

2.6 Summary of literature review

The main concept underlying this thesis is the use of the DPM monitoring method approved by the Mine Safety and Health Administration, which consists in collecting air samples. From the monitoring the DPM, total carbon could be defined, as is represented at 80 percent in DPM. Moreover, the total carbon is similar to the representation of elemental carbon, as it during combustion process, elemental carbon emissions are part of the DPM. Diesel engine characteristics influence the consistency of elemental carbon, and DPM accounts for about 80% of the overall quantity of elemental carbon in the atmosphere. During underground mining, diesel engines are responsible for producing somewhere between 35% and 84% of the PM1 pollution. Since during this thesis, the PMs and black carbon values are obtained, as a result, from the DPM concentration values from them could be defined.

3. METHODOLOGY

3.1. Experimental Measurements Approach

For this study air velocity, particulate matter and black carbon concentration, and lund-disposal surface area data was acquired during field tip from the underground metal mine located in Eastern Kazakhstan region. These data were acquired during measurements were done at various points throughout the mine. Two measures are done directly in the crosscut, and the second two are at the drift (inlet and exhaust zones of air). The simple visual representation of the measurements area is on Figure 4 (blue and pink lines are measurements area frames). Additional data was received from area under the end of auxiliary duct (2m, black lined).

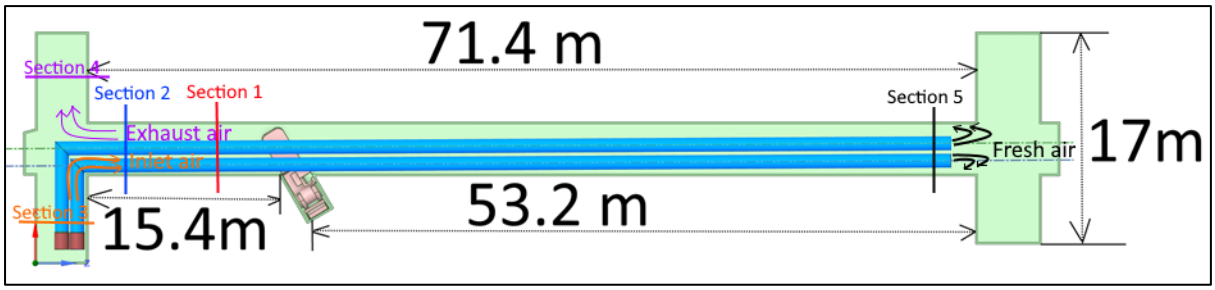

Figure 4. Simplified layout of the measurements area.

The measurements were done using tools: Naneos Partector 2, Microaeth, RizgardPM, and TSI ALNOR anemometer. During measurements, one LHD was operating as usual. At the day 1, the measurements are done at 5.5m and 14.45m (blue lines at Figure 5) far from operating LHD. For the day 2 (pink lines at Figure 5), the measures are done at 4.7m (inlet air), and 5.6m (exhaust air). The last day measurements were done at the end of drift – 2m from auxiliary duct (black lined). Measurements ssections are conventionally marked as, drift measurements: 5.5m from LHD (section 1), 14.45m from LHD (section 2), 2m from duct (section 5); cross cut measurements: 4.7m inlet air (section 3), and 5.6m exhaust air (section 4). Figure 5 below shows a 3D representation of the LHD location as well as the area (sections) where the measurements were made (Ansys software).

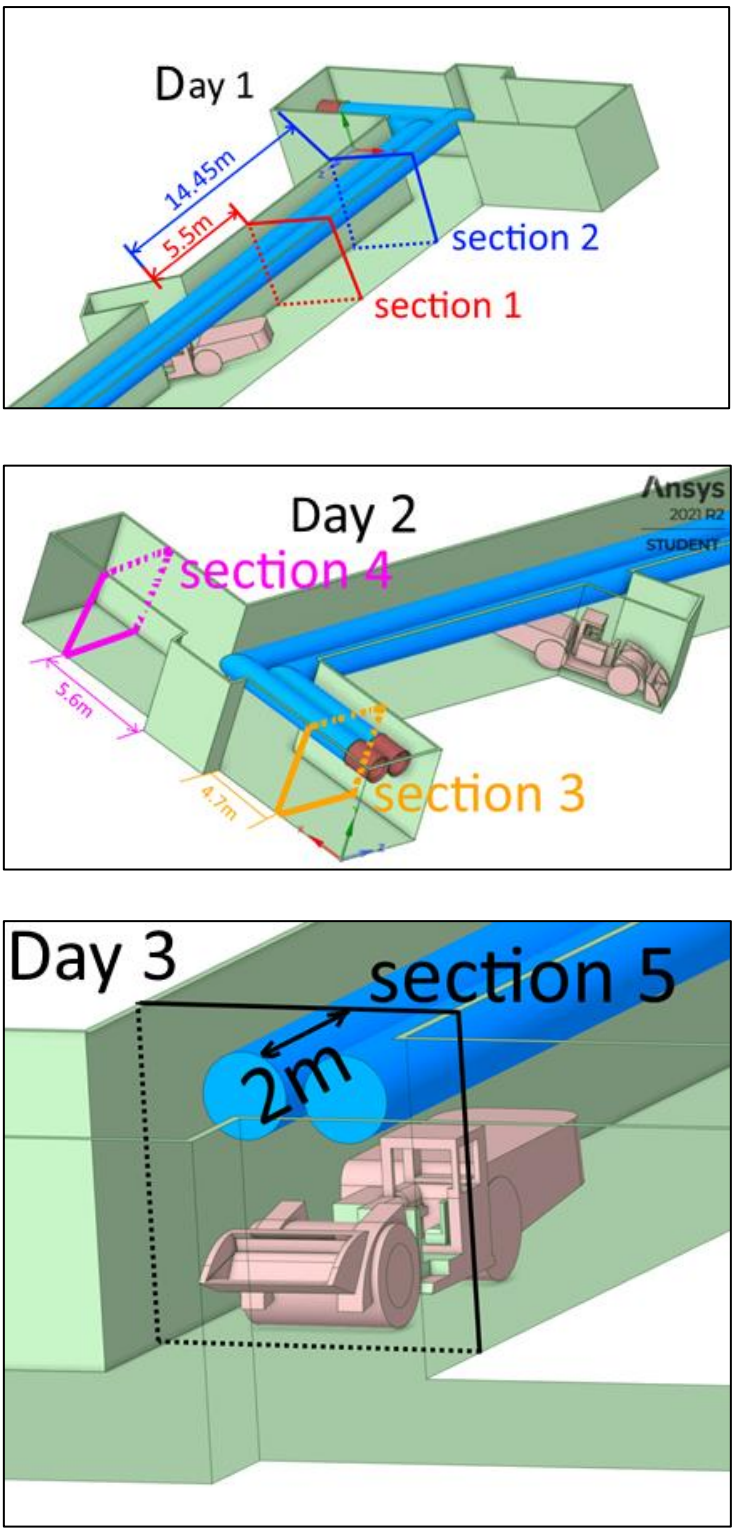

Figure 5. Location of LHD and measures distance, Day 1, Day 2 and Day 3.

The analysis of current thesis is focused on 5.5m and 14.45m distance from operating LHD (Figure 5). In the figure 6, distances 3-day measures differently colored and have proper sections. The measurements were carried

out at 9 points of cross section. Figure 6,

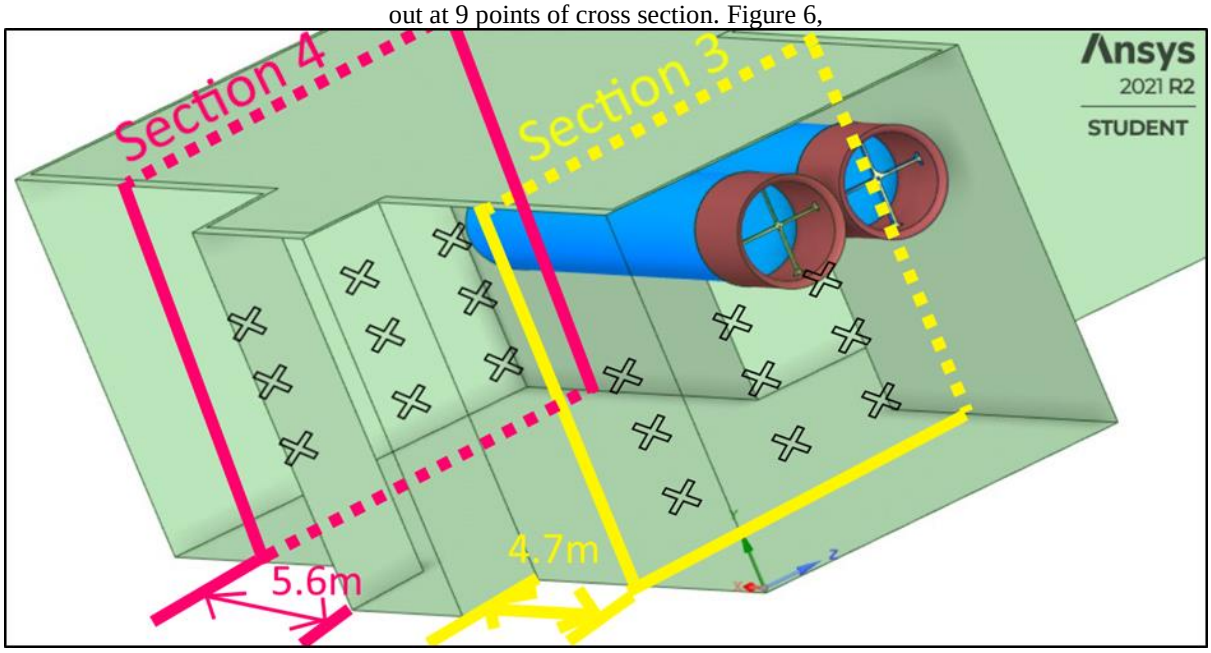

Figure 7, Figure 8 below shows a 3D view of these measurements.

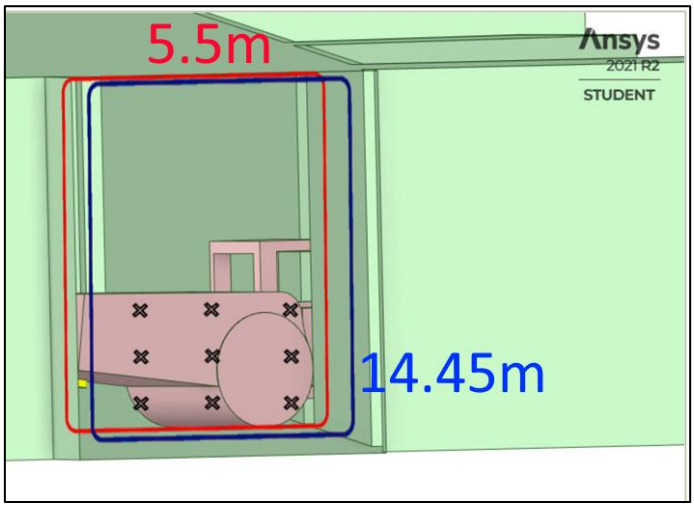

Figure 6. 3D view of measuring points, Day 1.

3D view of the Day 2 measurements points is given at

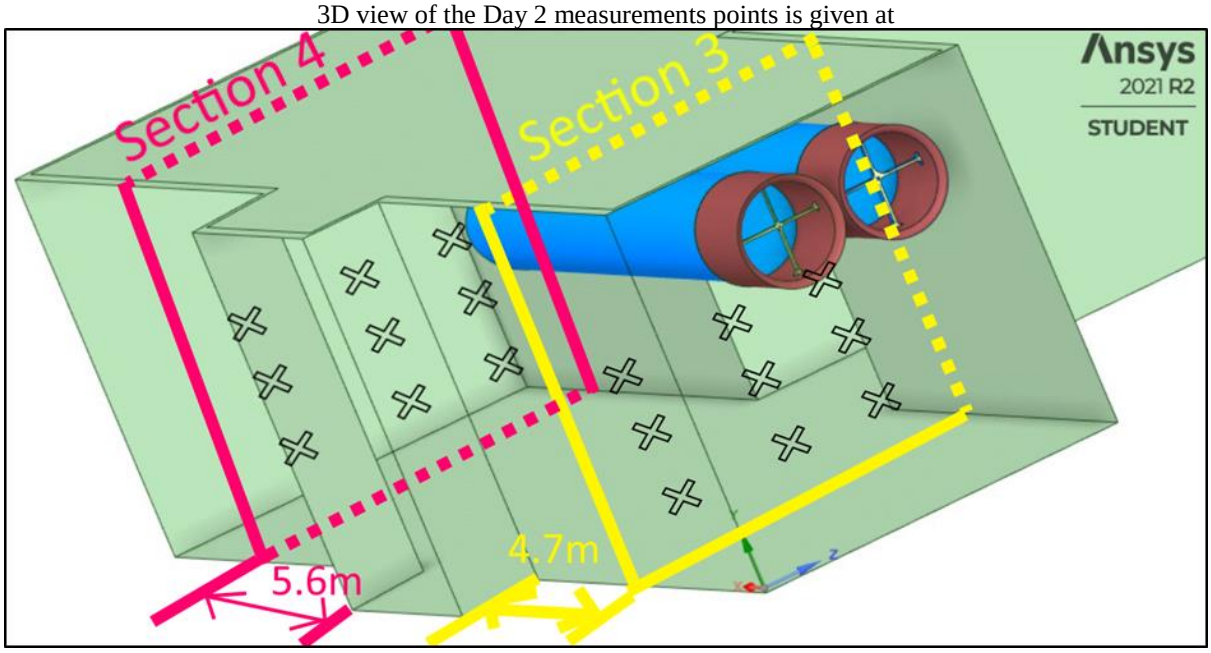

Figure 7. The measures of inlet air are (4.7m) provided at

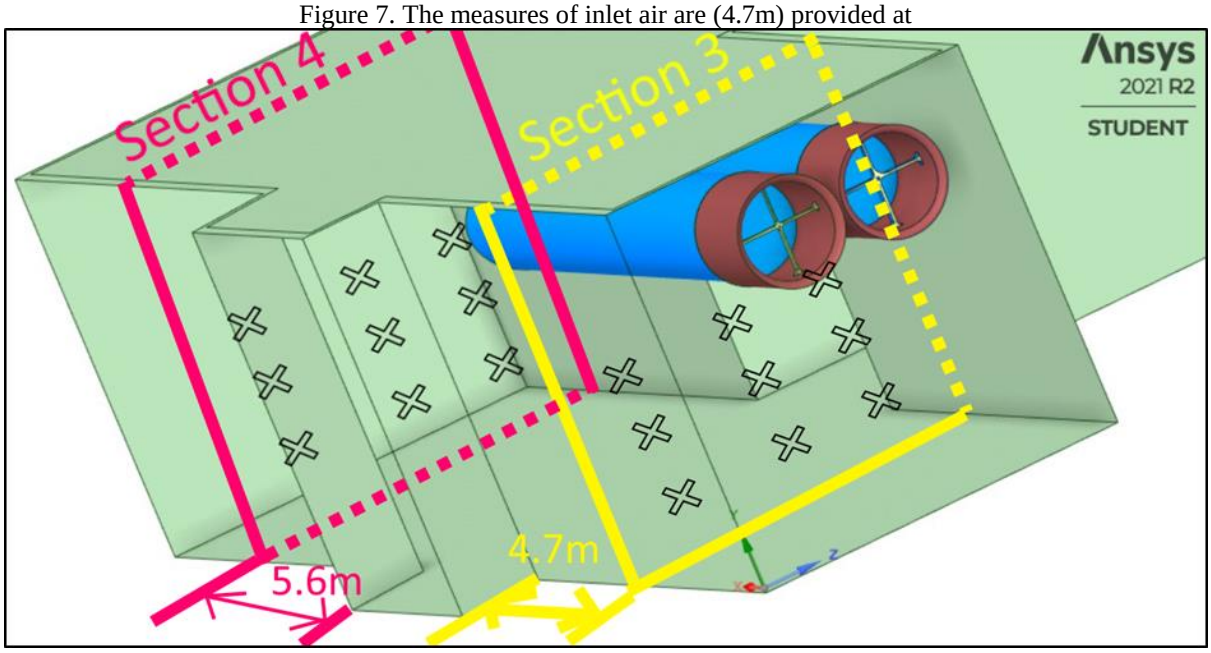

Figure 7 and yellow colored. Also, at this figure, the measures cross section of exhaust air (5.6m) are pink colored. Both these measures are done at the drift.

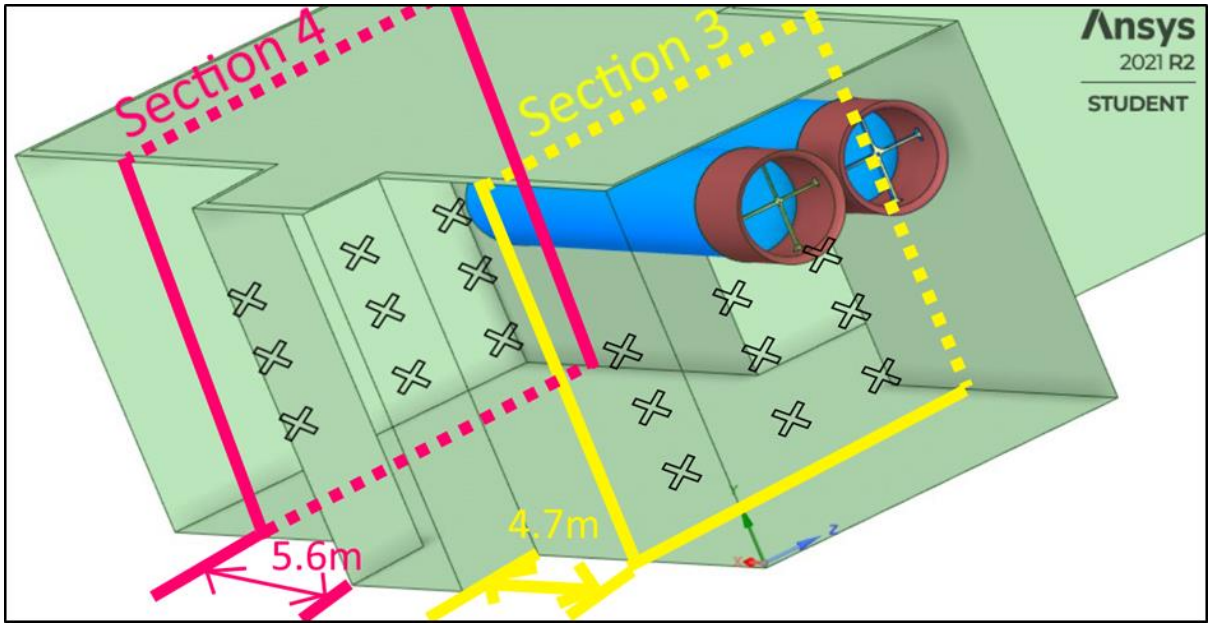

Figure 7. 3D view of measuring points, Day 2.

On Figure 8 shows nine points where measurements were taken from a distance of 2m from a duct, close to ore heading zone.

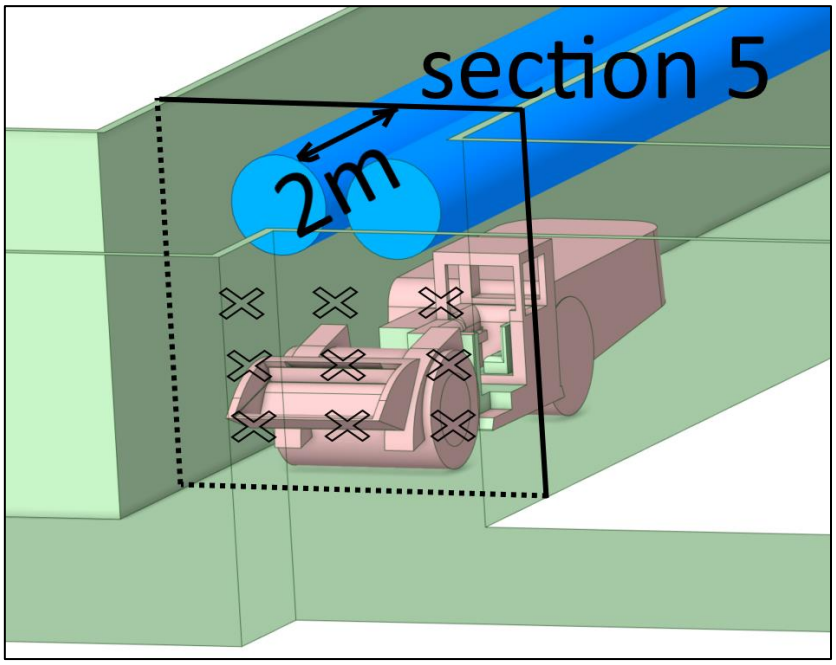

Figure 8. 3D view of measuring points, Day 3.

Next Figure 9, shows the distances between points, as well as two auxiliary ventilation ducts.

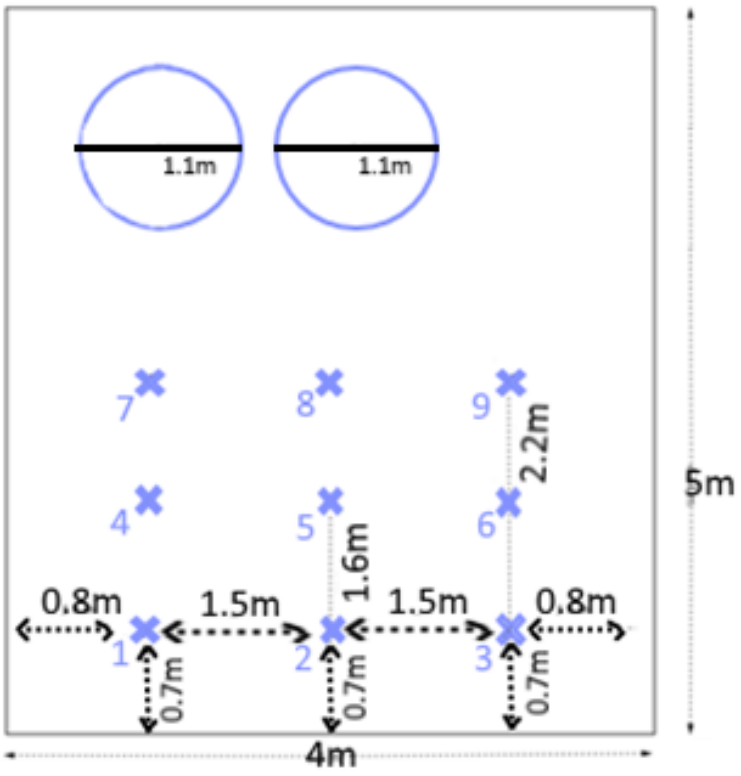

Figure 9. Schematic distribution of points of all sections of measurements.

The visual representation in Figure 9 shows the distribution of 9 points that were selected from the place where the measurements were carried out. In addition, Figure 10 shows the measurement process of the researchers directly in an underground mine.

Figure 10. Researchers in the mine.

The auxiliary fan that is connected to the duct is ‘ESN 9-450’. From the official distributor website, this auxiliary fan has characteristics: Volume flow up to 18.8 m^3/s; Total pressure increase up to 3000 Pascal; Motor shaft output 45 kW; auxiliary ventilation. In that particular case, considering the diameter of auxiliary duct, the drift velocity is 17 m/s.

After setting the auxiliary duct, an important parameter is to configure the LHD (CAT R1700 loader). Dimensions of LHD were taken from the official distributor website. Considering dimensional parameters, the geometry of the LHD truck is established (pink colored at Figure 11). An important parameter for DPM dispersions is location of the exhaust pipe. Exhaust pipe’s location is important in order to set the source of gaseous contaminants. Moreover, the geometry contains the exhaust pipe of a LHD (yellow colored) under the engine bay, right after the turbine.

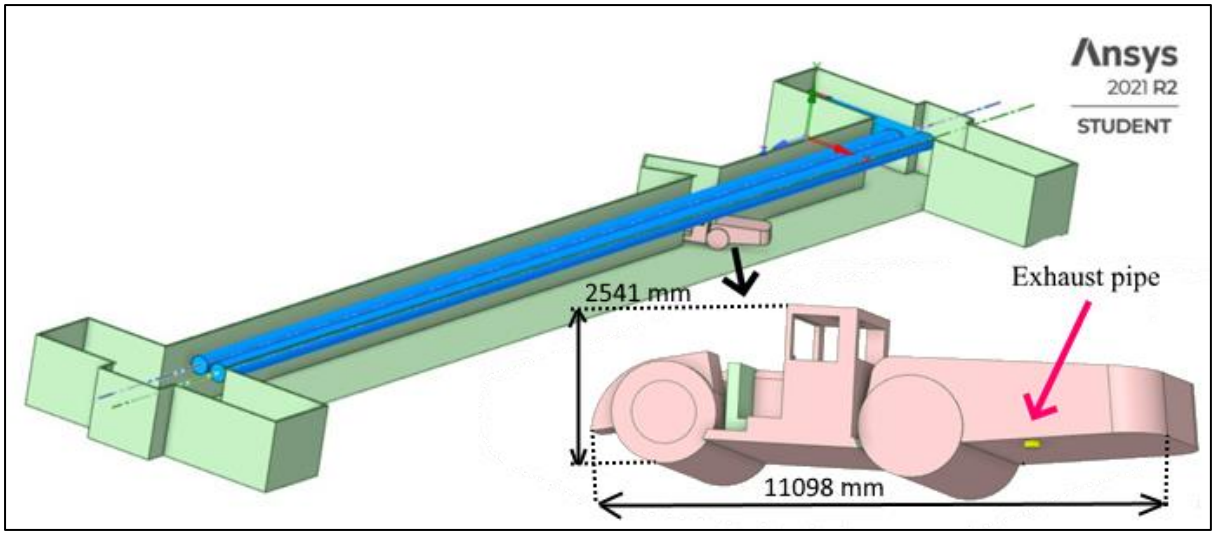

Figure 11. 3D model of underground drift and LHD.

Continuous exposure to exhaust gases depends on the geometry of the underground mine. Important parameters included in geometry are auxiliary ventilation duct, exhaust pipe of mine truck, and the dimensions of the mine truck.

3.2. Sampling instrumentations

The research is carried out on equipment provided by Nazarbayev University. Four instruments that were used:

- RigzardPM Plus is a monitor for measuring particles with a diameter less than 1 micrometer;
- Microaeth MA200 - monitor measuring the concentration of black carbon;
- Naneos Partector 2 is a monitor for the analysis of small particles presumably deposited in the lungs;
- TSI ALNOR ROTATING VANE RVA501 is an anemometer with the function of determining volume, velocity and temperature.

According to Partector 2 developers, this device is the world's smallest multimeric nanoparticle detector. Dual non-contact detection stages are used in the Partector 2 to measure not only the lung-deposited surface area (LDSA), but also the particle number concentration and the average particle dimension of the particles. Additionally, the surface area of ultrafine particles (UFPs) and the ultrafine particle mass concentrations are computed and available to present. Instead of estimating LDSA mass using a simple multiplier, UFP mass is determined by utilizing the measured diameter of the particles, according to the tool manufacturers. The

importance of this tool is due to the impact of nanoparticles on health. Thus, according to the findings of a Brown, Wilson, MacNee, Stone, and Donaldson (2001) research, the biological response is influenced by particle surface area. Nanoparticles may also be able to penetrate epithelial cells and enter the circulation of the lungs because of their tiny diameter (Kreyling, Semmler, Erbe, Mayer, Takenaka, Schulz, H., and Ziesenis, 2002), and as well as a route via which they may reach the brain through the olfactory nerves (Oberdörster, Sharp, Atudorei, Elder, Gelein, Kreyling, and Cox, 2004).

Another device, Microaeth MA200 is a black carbon-monitoring device. In order to do an absorption study at five wavelengths, this instrument measures the rate of light transmission through the filter (according to the tool manufacturers).

Additionally, RigzardPM Plus, which is a tool that measures particles with less than 1 micrometer in diameter (according to the tool manufacturers). Accurate particle matter concentrations have been ensured through calibration against reference aerosol sensors. This tool has been used to assess the impact of particulate matter on air quality and mine personnel (PM1, PM2.5, and PM10).

Moreover, TSI ALNOR ROTATING VANE RVA501 anemometer was used during underground measurements. This tool provided information of air velocity, air volume, and temperature in metric units. By using coils, diffusers, gratings, and filters to measure flows that are irregularly distributed or fluctuating, this anemometer is a useful tool (according to the tool manufacturers).

The data analysis using two techniques: Pearson linear correlation coefficient and coefficient of determination (R^2). With the use of an optimization criterion and the Pearson correlation coefficient, it is possible to choose the optimal noise reduction filters based on their correlation coefficient (Benesty, Chen, Huang, and Cohen, 2009). Moreover, the coefficient of determination measures “how well a regression model predicts a dependent variable from independent variables” (Nagelkerke, 1991). For the measured results, these analyzing techniques provide information of how one variable is dependent to the second one. For measured results, these analysis methods provide information about how one variable depends on the second. In particular, how exposure of PM1, BC are affected from velocity and temperature.

4. RESULTS

4.1 Mine Site Experimental Measurements

This study was conducted based on data from a field trip from September 21 to 23, 2021. The next subsections examine and show in further depth the analysis of the measurement results obtained using four separate instruments. Air measurements were carried out at depth +375 level.

4.1.1 First Day of Measurements

In this subsection, the results of the anemometer, Partector and RizgardPM tools are presented during the Day 1 of measurements. However, at the first day, the black carbon measurements have not been done. The visual representation of measurements area is given at Figure 12.

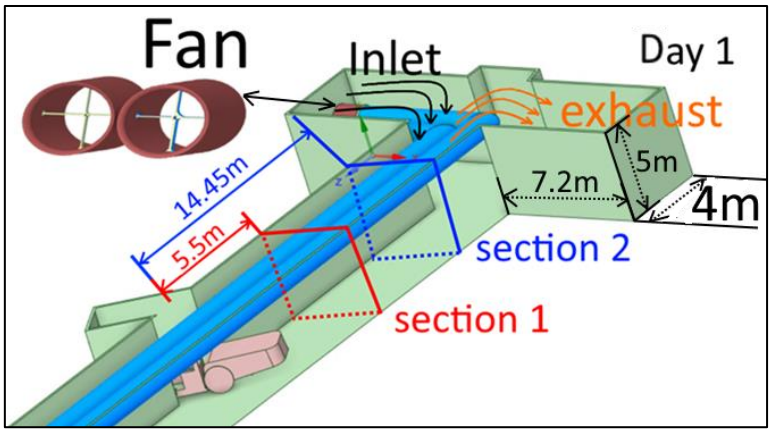

Figure 12. Measurements area of Day 1.

From the measurements, the results of the anemometer are averagely shown in Table 2. This table contain the results of air velocity and temperature from section 1 and section 2.

Table 2. Results of the anemometer, Day 1.

Date 21 Sep	Temperature, ℃	Airflow velocity, m/sec
Average	23	0.8

As a result, the anemometer of air velocity and temperature is achieved from total 18 minutes measures from two sections. Parallel to the velocity and temperature measurements, the average LDSA, as well as particle diameter data was achieved from use of Partector tool. This data is used for further correlation analysis. The measured average results of Partector are at Table 3.

Table 3. Results of the Partector, measuring Day 1.

Date 21 Sep	**Diameter, nm**	**LDSA, µm²/cm³**	**Surface area concentration µm²/cm³**	**concentration, µg/m³**
AVERAGE	100	4300	52000	3000

From the findings, the average diameter during measures is 101.64 nm. That correspond to LDSA exposure of 4299.16 µm²/cm. In addition to these tools, by using the RizgardPM, it was able to obtain different PM values. And they averaged values are at Table 4.

Table 4. Results of the RizgardPM, Day 1.

Date 21 Sep	**PM1, µg/m³**	**PM2.5, µg/m³**	**PM10, µg/m³**
AVERAGE	650	1350	1650

From the use of the RizgardPM tool, the different particles (PM1, PM2.5, and PM10) diameters concentrations are defined. As a result, referring to the results of the first day of measurements, LDSA relationship to velocity and temperature data are interpreted in Figure 13. Black line divide results in to two: 12:23 – 12:49 PM are for Section 1 results, and Section 2 results are from 1:03 – 1:33 PM.

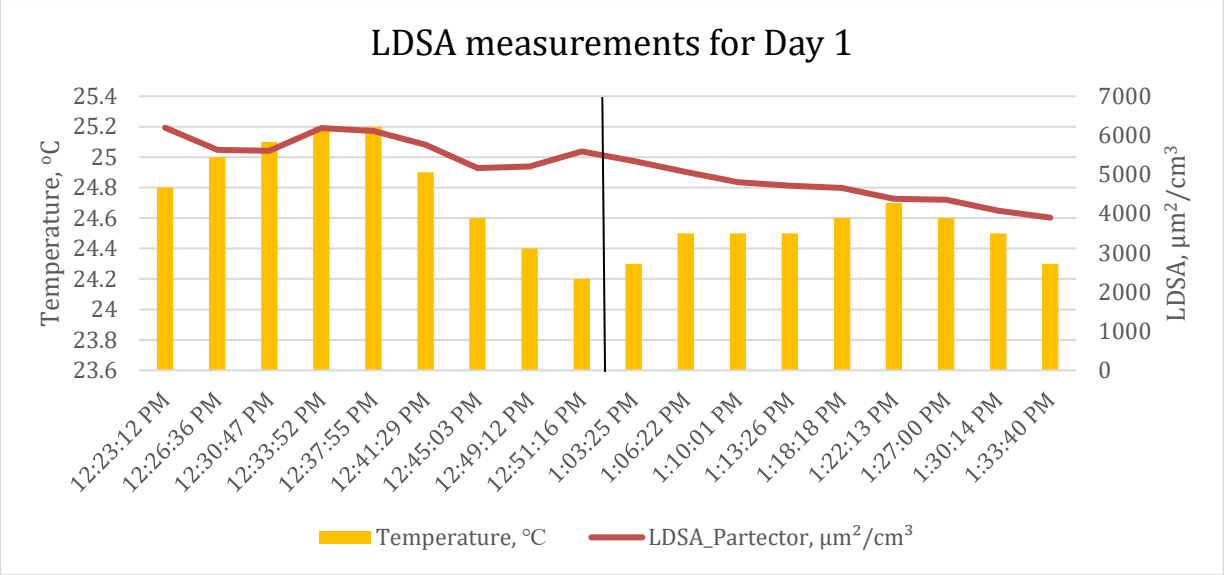

a) LDSA results in relation to temperature.

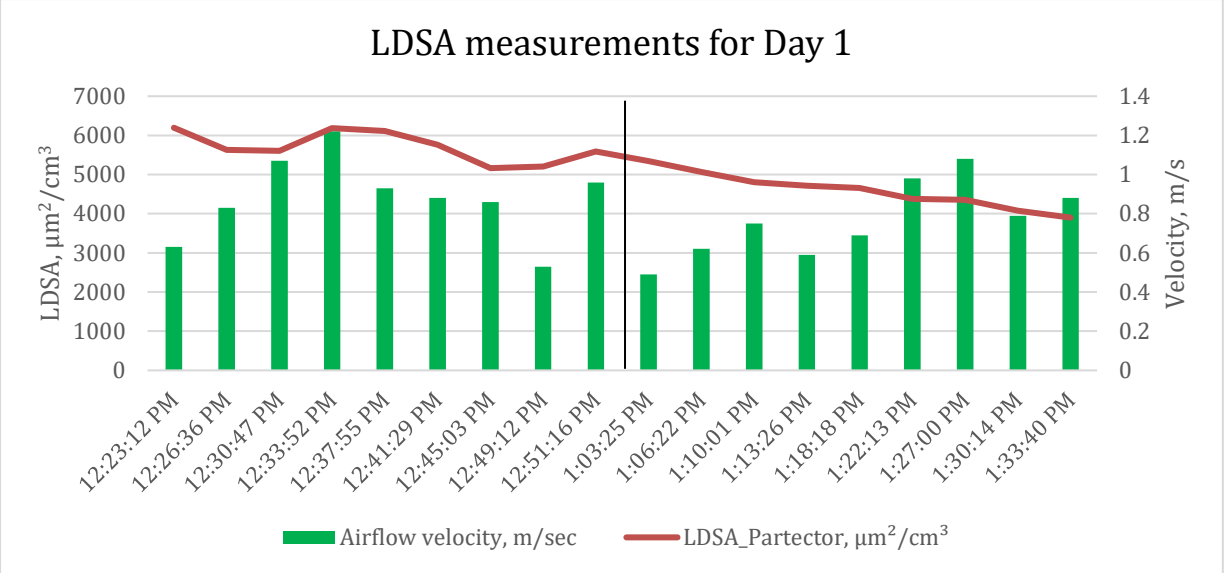

b) LDSA results in relation to velocity.

Figure 13 a, b. Values of anemometer compared to LDSA, Day 1.

According to the visual assessment of Figure 13 a and b, when air velocity is measured, the LDSA is shown to be inversely proportional. This trend is seen during 12:26-12:37 PM, as well as from 1:22 to 1:33 PM. Next Figure 14 shows the results of PM measurements in relation with temperature and air velocity.

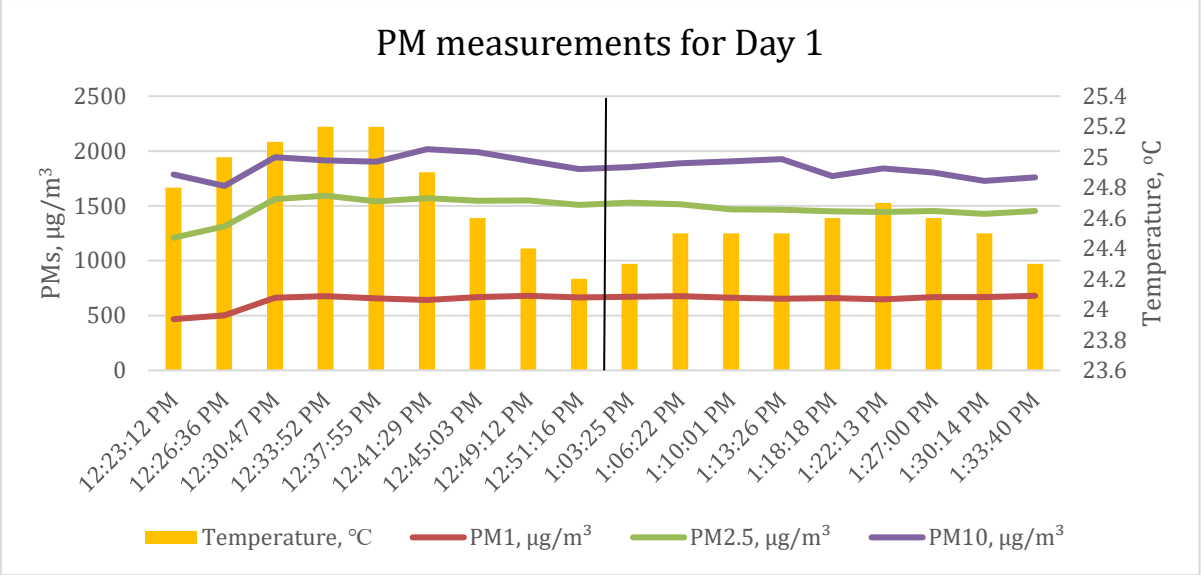

a) PM results in relation to temperature.

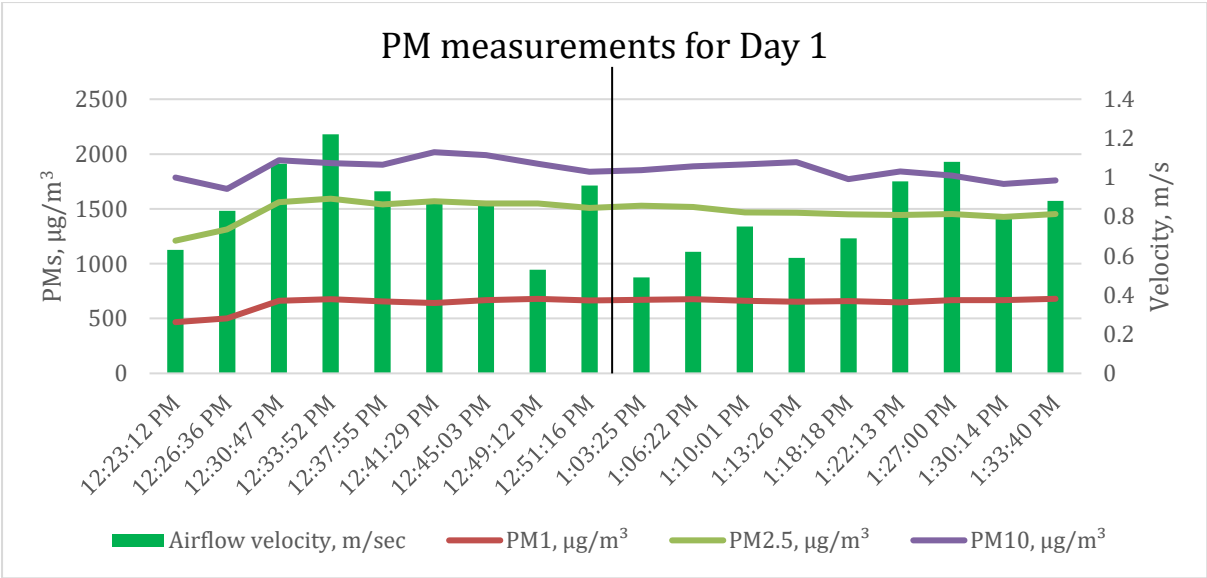

b) PM results in relation to velocity.

Figure 14 a, b, c. Values of anemometer compared to PMs, Day 1.

Figure 14 shows that the air is related to the effects of PM. From 12:26 to 12:41 PM measurements, the different PM values are tending to reduce as a result of air velocity growth. In addition, this trend is observed at the beginning of measurements and from 13:12 to 13:18 PM at the Section 2.

4.1.2 Second Day of Measurements

For the Day 2 measurements, velocity, temperature, LDSA, PMs, and BC values are received using anemometer, Partector, RizgardPM, and Microaeth. Figure 15 below depicts the area from where, the measures were done: Section 3 correspond to measures under air inlet, and Section 4 are measures of exhaust zone.

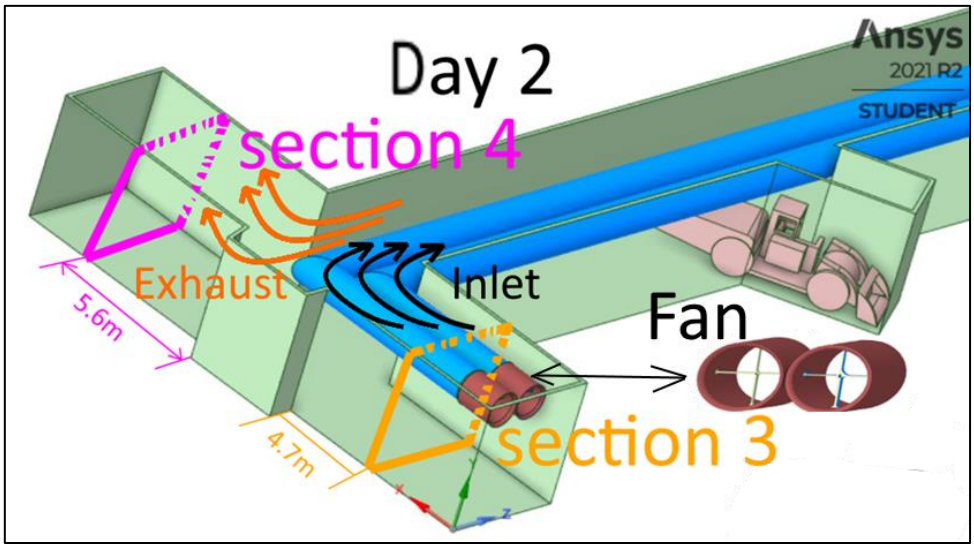

Figure 15. Measurements area of Day 2.

Using available data, Table 5 shows the average anemometer findings from the Day 2 of measurements. These values correspond to the average temperature and velocity in the cross-cut.

Table 5. Results of the anemometer, Day 2.

Date 22 Sep	**Temperature, ℃**	**Velocity, m/sec**
AVERAGE	23	0.9

Additionally, the data of Partector on the Day 2 measurements are given at Table 6. The data consist the average LDSA exposure, and particle diameter values.

Table 6. Results of the Partector, Day 2.

Date 22 Sep	**Diameter, nm**	**LDSA, µm²/cm³**	**Surface area concentration µm²/cm³**
AVERAGE	90	3700	4200

From the findings of Day 2 Partector tool measures, the average particle diameter is 89.55 nm, and that correspond to average LDSA exposure of 3680.64 µm²/cm³. Additionally, the RizgardPM instrument produced the data given in part in Table 7 on the Day 2 of measurement.

Table 7. Results of the RizgardPM, Day 2.

Date 22 Sep	**PM1, µg/m³**	**PM2.5, µg/m³**	**PM10, µg/m³**
AVERAGE	580	950	1100

From the findings of RizgardPM tool, the average PM1, PM2.5, and PM10 values are achieved. In addition, by using Microaeth tool, black carbon concentration is measured. And according to the results, the average black carbon concentration during measurements is 2423.86 µg/m³.

Similar to the analysis of the first day, the values of the anemometer and PM are visually plotted in Figure 16. Visually, Day 2 measurements results are divided with black line. The black line corresponds to results from 12:21-12:29 PM (section 3), and 12:30-12:38 PM (section 4).

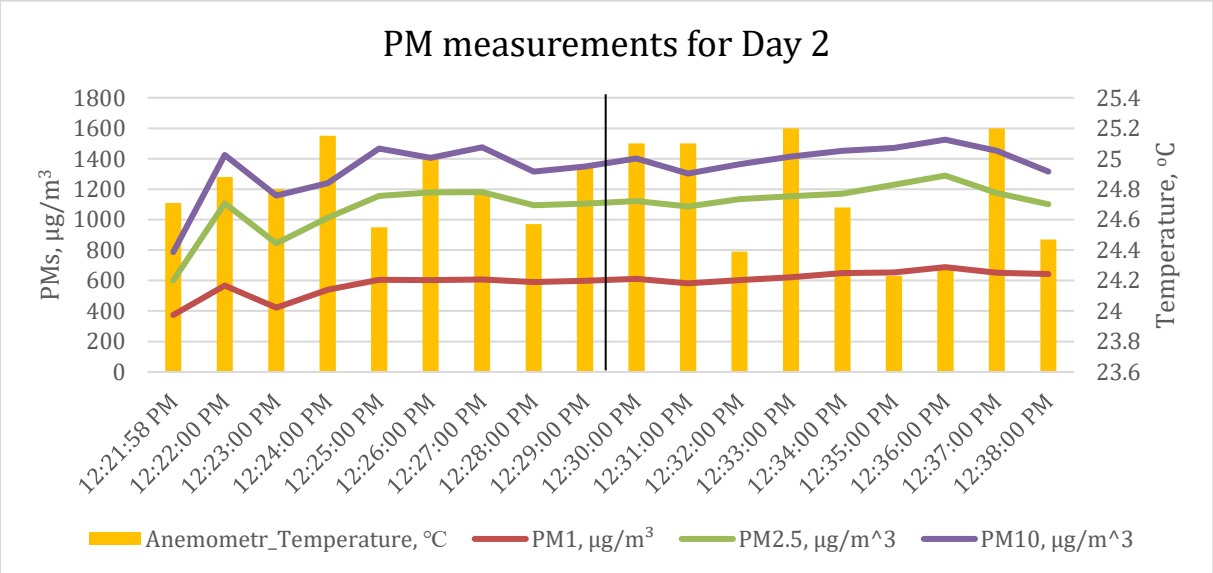

a) PM results in relation to temperature.

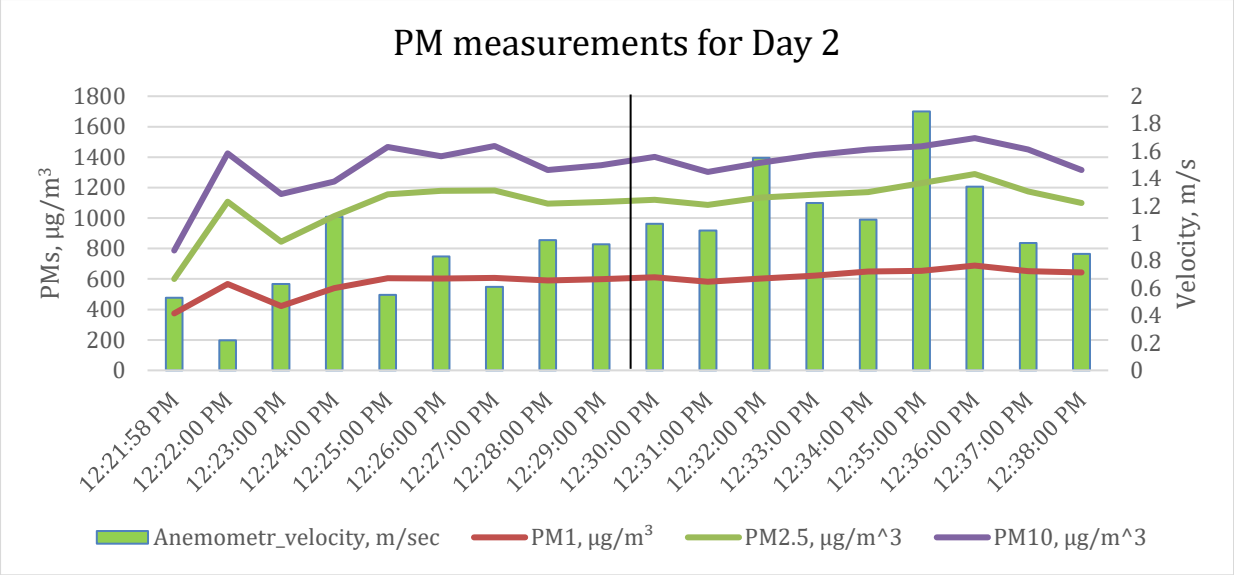

a) PM results in relation to velocity.

Figure 16 a, b. Values of anemometer compared to PMs, Day 2.

The Day 2 of measurements reveals the same pattern as the first day of measurements. During low velocity period, the exposure of PM is high. This tendency is seen from 12:22-12:29 PM. Using data from Partector and anemometer tools, Figure 17 below shows the LDSA exposure in relation to air temperature and velocity.

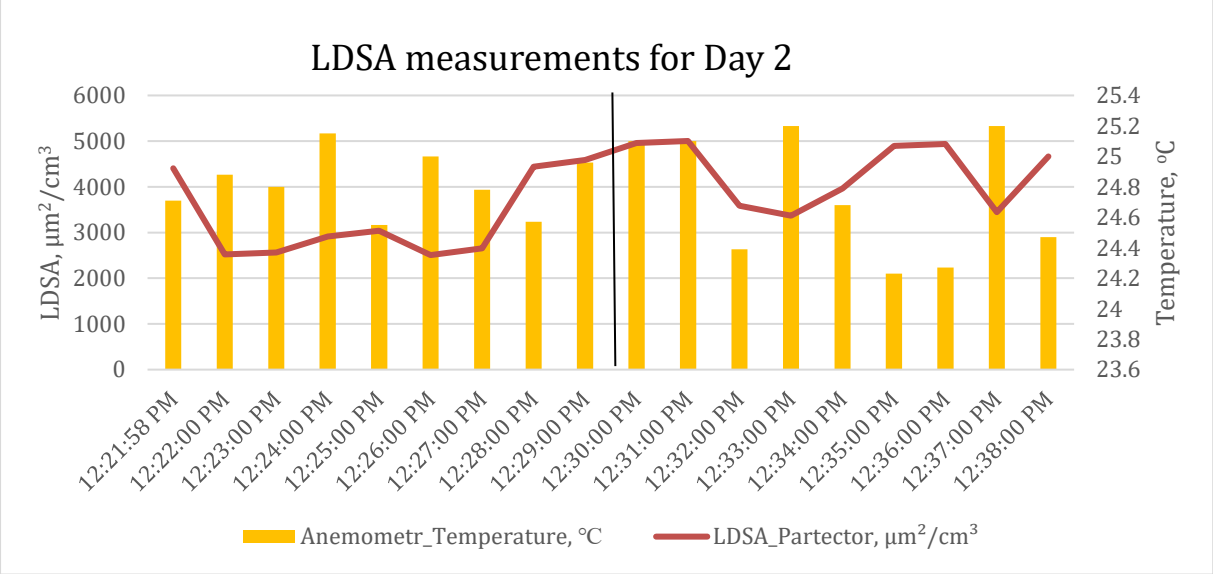

a) LDSA results in relation to temperature.

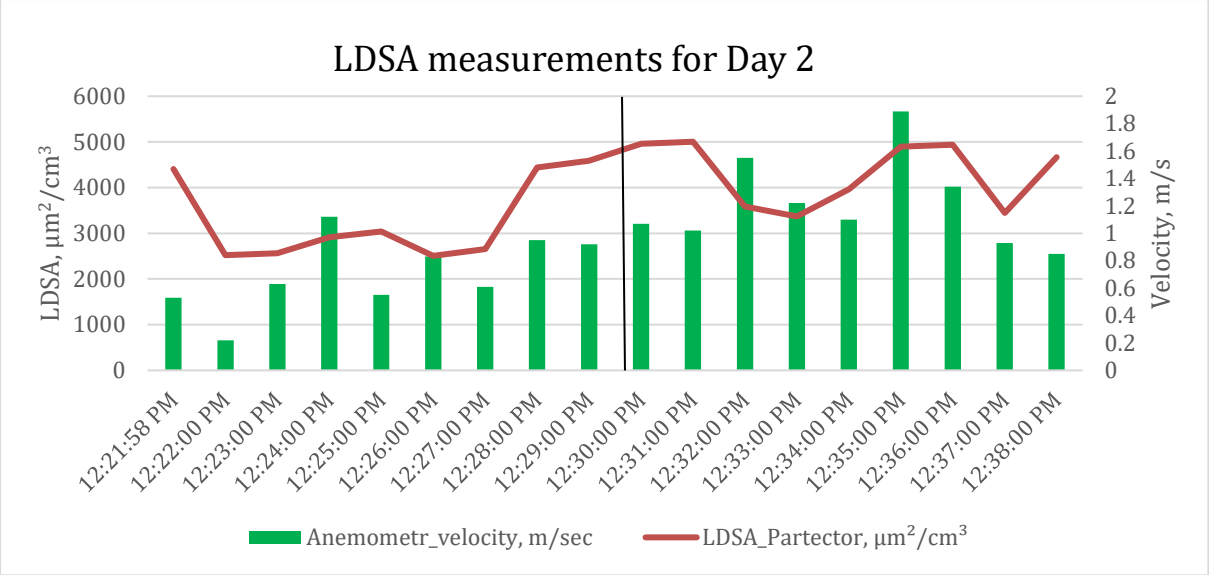

b) LDSA results in relation to velocity.

Figure 17 a, b. Values of anemometer compared to LDSA, Day 2.

From the Figure 17, the increase of LDSA exposure is associated with reduced air velocity. However, the temperature has opposite way, and increase of LDSA is during air temperature growth. Both trends is seen during 12:27-12:32 PM sampling period. In addition to that, using air velocity and temperature data, the black carbon concentration (Microaeth tool) values is given at Figure 18 below.

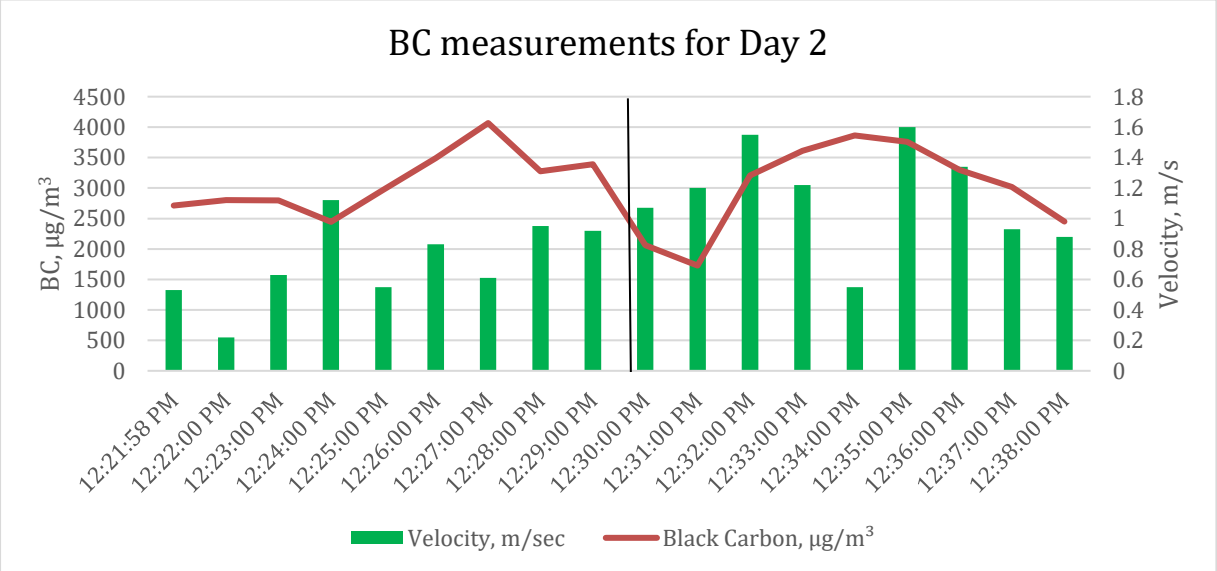

a) BC results in relation to velocity.

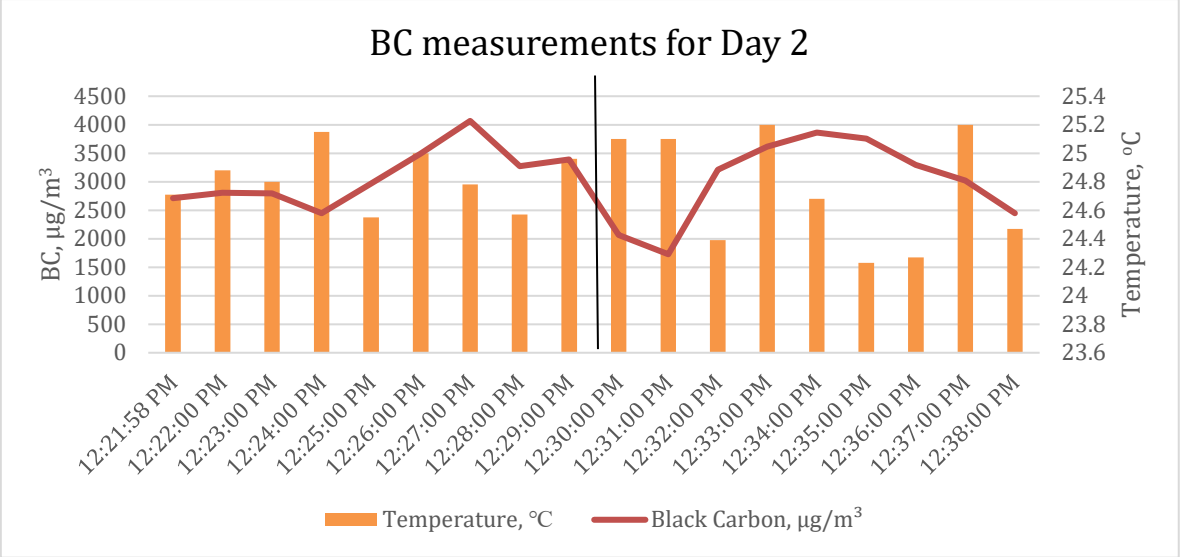

b) BC results in relation to temperature.

Figure 18. Values of anemometer compared to BC concentration, Day 2.

According to Figure 18, the trend of low velocity is seen during 12:25-12:29 PM. Moreover, during 12:33-12:36 PM, the lowered temperature trend is seen. During that time the growth of black carbon concentration is observed during the low air velocity. Same, as velocity, the period of low temperature is associated with increased black carbon concentration.

4.1.3 Third Day of Measurements

Results of the anemometer, Partector, and Microaeth tools are presented during the Day 3 of measurements (Figure 19). From these tools, the air velocity, temperature, LDSA, and black carbon concentration data is achieved.

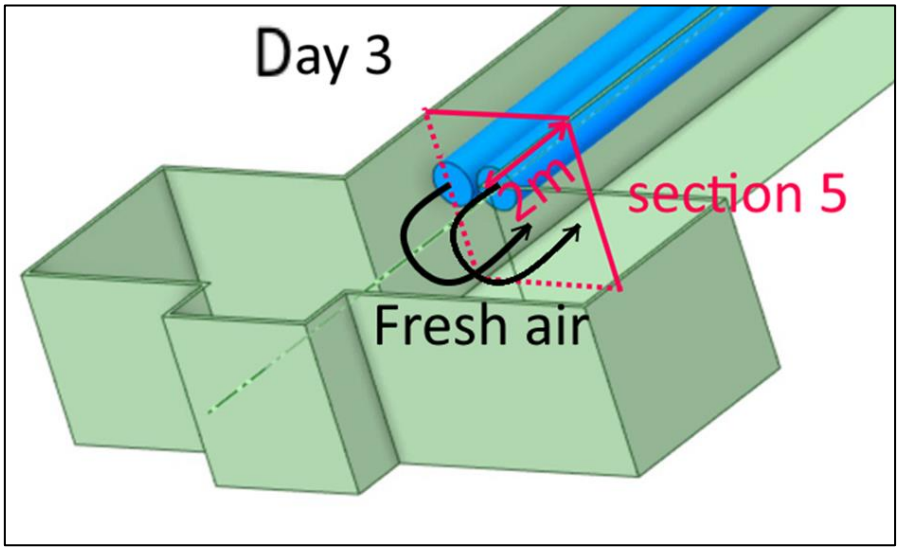

Figure 19. Measurements area of Day 3.

According to the achieved results, the Table 8 shows average temperature and velocity readings from anemometer tool.

Table 8. Results of the anemometer, Day 3.

Date 23 Sep	Temperature, ℃	Velocity, m/sec
AVERAGE	24	0.5

In addition to the anemometer data, according to Partector tool, the average diameter and LDSA exposure is revealed (Table 9).

Table 9. Results of the Partector, Day 3.

Date 23 Sep	Diameter, nm	LDSA, µm²/cm³	Surface area concentration µm²/cm³	concentration, µg/m³
AVERAGE	110	3900	48000	3300

From the Table 9 results, the average particle diameter is 108.29 nm. This value correspond to average 3866.26 µm²/cm³ LDSA exposure. In addition to that, the measurements using the Microaeth instrument, revealed average black carbon concentration, which is 2489.64 µg/m³.

Graphical representation of available data from Day 3 are visually interpreted at figures below. For the last, two measurements at the same section 5 were done. Following figures correspond to the results achieved after measurements.

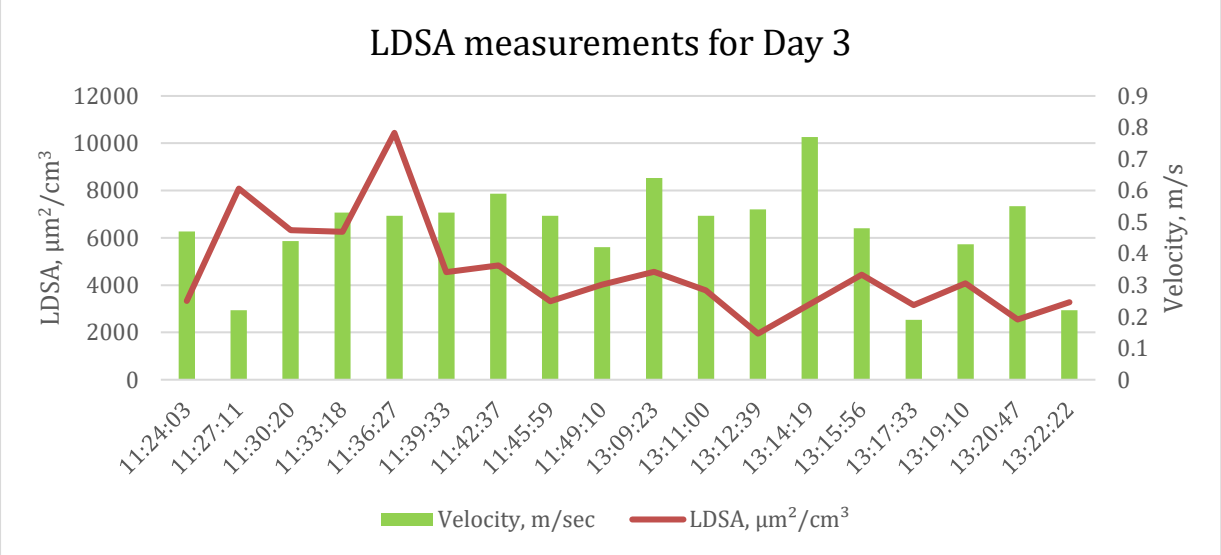

a) LDSA results in relation to velocity.

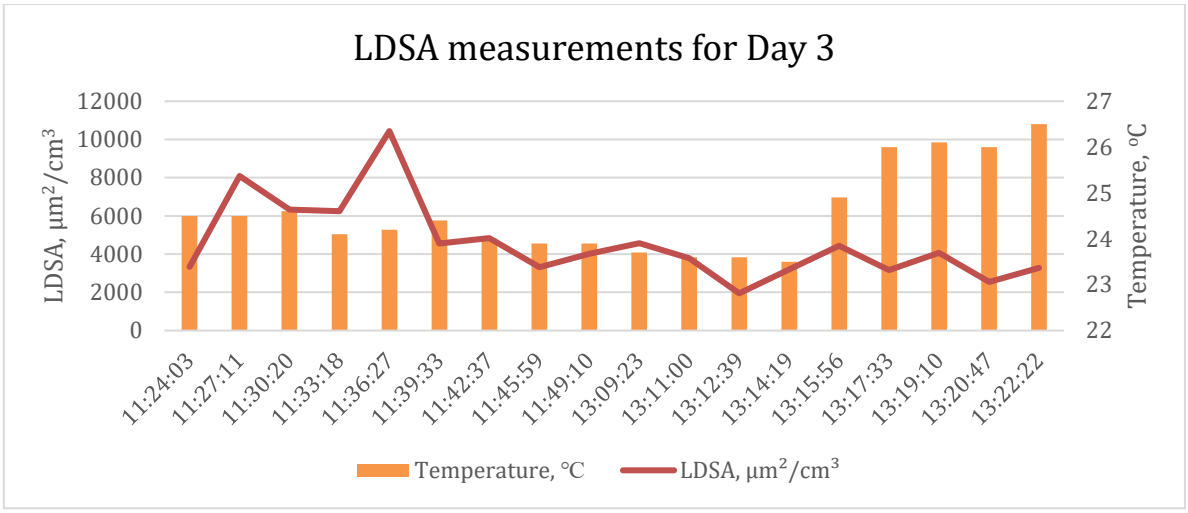

b) LDSA results in relation to temperature.

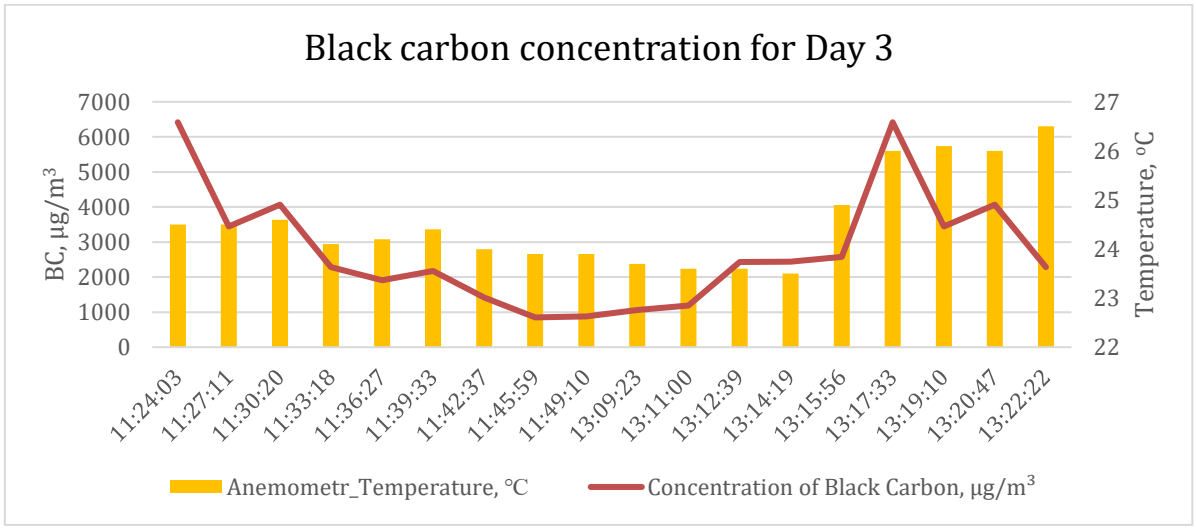

c) BC results in relation to temperature.

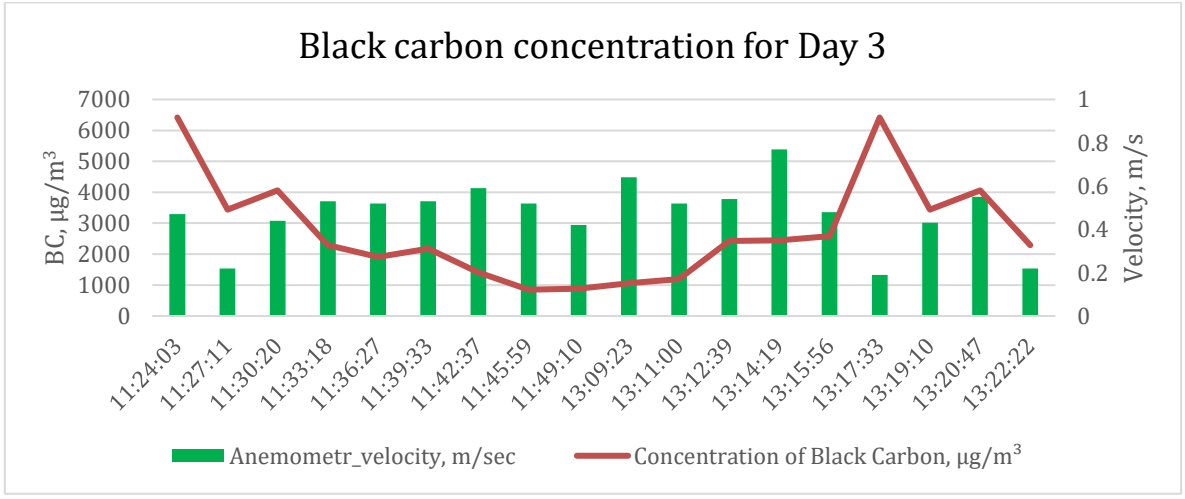

d) BC results in relation to velocity.

Figure 20 a, b, c, d. Values of black carbon concentration and LDSA compared to anemometer values, Day 3.

From the Figure 20, the black carbon concentration and LDSA exposure in relation to velocity and temperature are adapted. From the findings, the lowered LDSA exposure associated with increased air velocity. This trend is seen from 11:39-11:46 AM, and 1:09-1:15 PM. Same as velocity, the increased temperature from 1:15-1:22 PM lead to LDSA reduction. Moreover, during 11:36-11:49 AM, an increased velocity lead to drop of black carbon concentration. However, the temperature during that period was low.

4.2 Received Data Analysis

4.2.1 PM1, BC, And LDSA to Velocity Correlations

Day 1

A three-day sample session indicated the current underground mining conditions. The effects of PM1, BC and LDSA, have been shown to be considerable. Further data analysis is performed as the degree of linear correlation of two variables using the excel trendline function. In addition to that, for finding the linear correlation, the Pearson Correlation Coefficient (PCC) function is chosen (Benesty et al., 2009). This coefficient shows three correlations: negative, zero, and positive (the value range between -1 to 1). Next figures represent the plot from available data and PCC.

For the first day of measurements, the linear correlation between PM1 concentrations and air velocity is given at Figure 21. This data is taken by use of anemometer and RizgardPM tools.

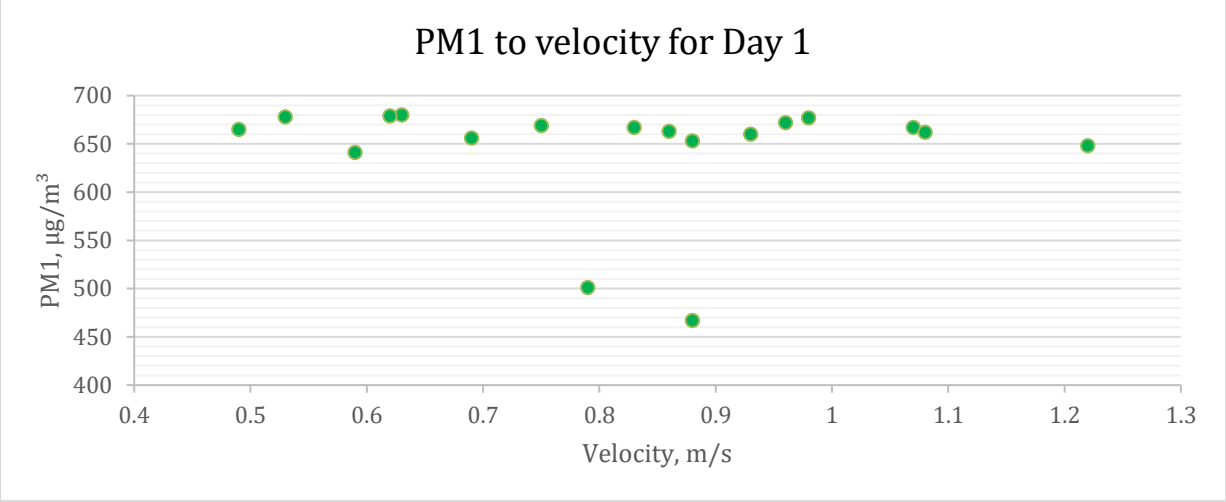

Figure 21. Air velocity to PM1, Day 1.

The Figure 21 depicts the data of air velocity and PM1 concentration. In addition to that, the $PCC = -0.07$, thus the negative correlation is observed. That mean that, there would be slight decrease of PM1 results in growth of velocity. Using data from Partector and anemometer tool, next Figure 22 shows analysis of LDSA values and air velocity (Day 1).

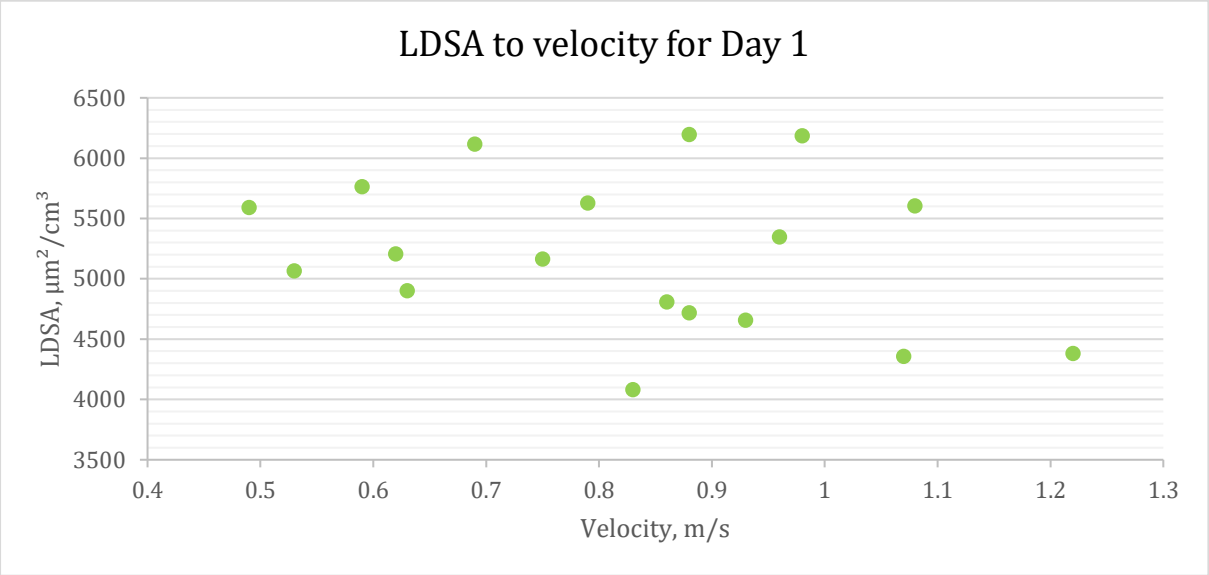

Figure 22. Air velocity to LDSA, Day 1.

The results of Figure 22 include data of LDSA and air velocity. In addition, the LDSA and values have negative trend ($PCC = -0.27$). Thus, the minor lung exposure growth is associated with decreased air velocity.

Day 2

As for Day 2 data, the same procedure. Using data of Microaeth and anemometer tool, the Figure 23 depicts air velocity values association with black carbon concentration (Day 2).

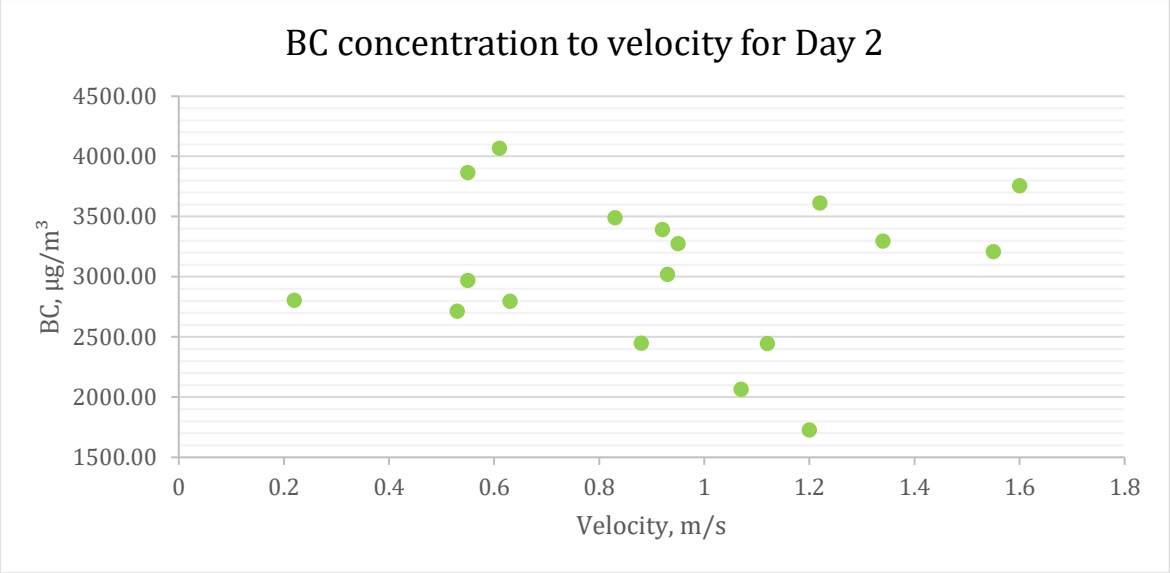

Figure 23. Air velocity to black carbon concentration, Day 2.

From the Figure 23, the values of velocity and black carbon shown. The confirmation is from PCC, where this factor showed negative correlation (-0.01). As the correlation is almost zero, the small decrease of black carbon due to increased velocity. Next Figure 24 depicts the plot between LDSA and velocity for Day 2. This data is taken from Partector and anemometer tools.

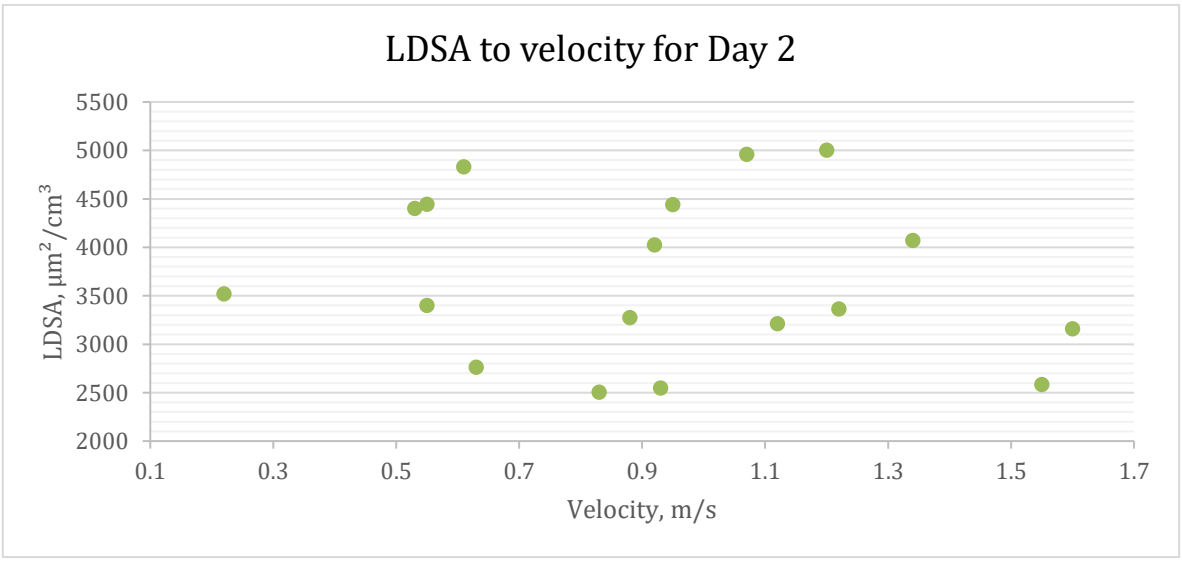

Figure 24. LDSA exposure to velocity, Day 2

From the Figure 24, velocity and LDSA exposure are given. In addition to that, the PCC has a negative correlation (-0.15). Using data of velocity, the plot between it and PM1 concentration is visually presented at Figure 25.

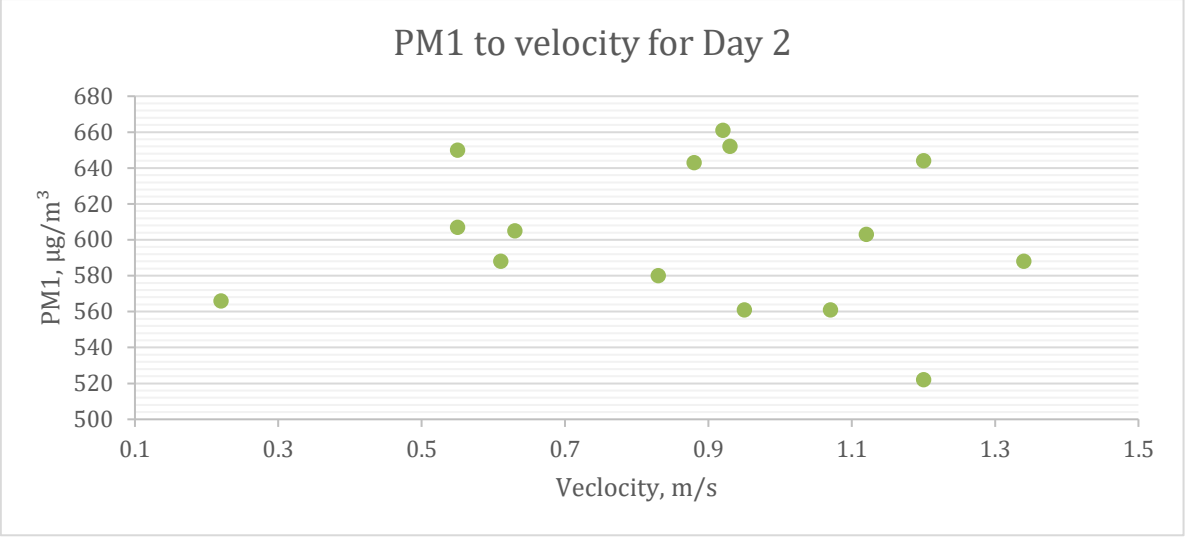

Figure 25. PM1 to air velocity, Day 2.

The visual assessment of Figure 25 shows association between velocity and PM1 concentration. In addition to that, the PCC coefficient is negative, but low, and equal to -0.078. Thus, the growth of velocity will lead to small PM1 drop. For the Day 3, using data of velocity, the data of between it and BC concentration is visually presented at Figure 26. This data is taken from anemometer and Microaeth tools.

Day 3

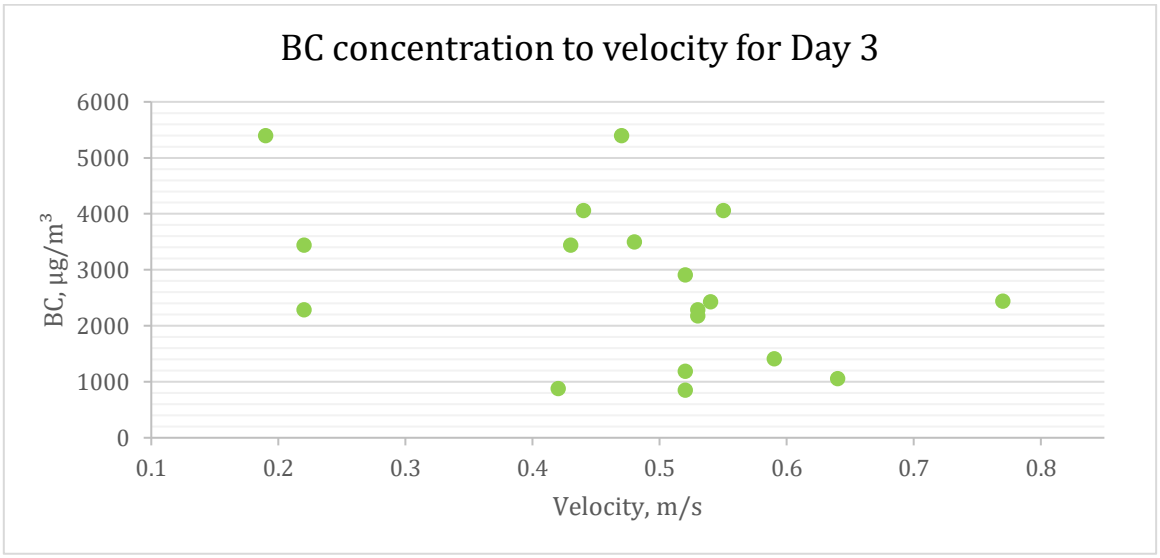

Figure 26. Air velocity to black carbon concentration, Day 3.

From the Figure 26 the data of air velocity interpreted to black carbon concentration. Moreover, after use of PCC, where this factor shows negative correlation and it is equal to -

0.4. In addition to that, using data from anemometer and Partector tools, next Figure 27 shows air velocity values compared to LDSA.

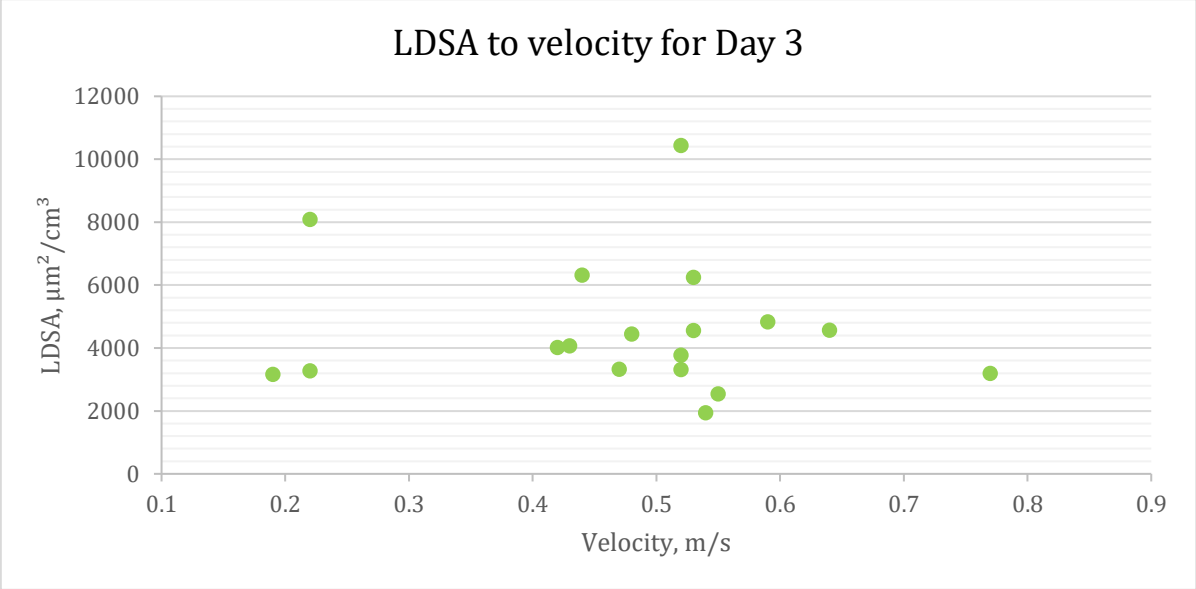

Figure 27. Air velocity values to LDSA, Day 3.

From the Figure 27, the observations are almost same as for first day measurements, and negative correlation is observed. This is because, the $PCC = -0.4$ between LDSA exposure and air velocity. Thus, the decrease of LDSA are resulted due to increased air velocity.

4.2.2 Regression Analysis Between Different Instrumentations

In this subsection, the combined data from Day 1 and Day 2(BC and PM1, LDSA and PM1), as well as Day 2 and Day 3 (LDSA and BC) is used. The BC concentration data is taken from Microaeth tool, PM1 data is measured using RizgardPM tool, and LDSA exposure is taken from Microaeth tool. Considering LDSA and PM1 concentration values the plot below represents the available data between these factors (Figure 28).

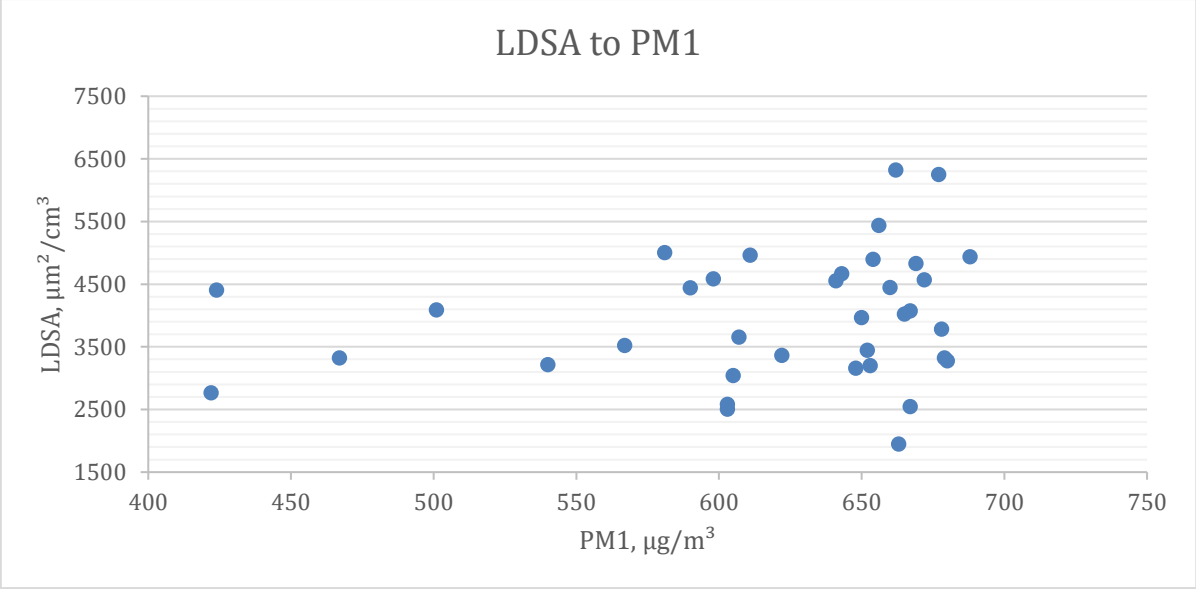

Figure 28. LDSA to PM1, combined.

The data from Figure 28 shows an association between PM1 and LDSA exposure. In addition to that, the $PCC = 0.2$ between LDSA and PM1. Next figure, considering LDSA and BC concentration values (Figure 29).

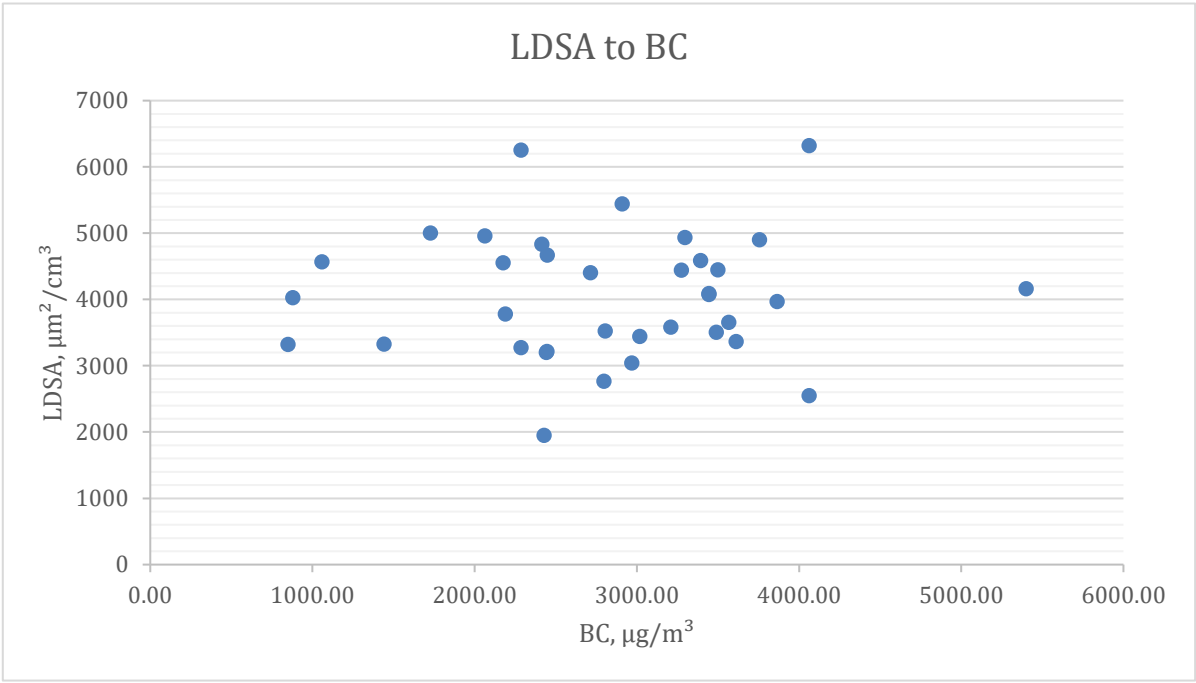

Figure 29. LDSA to BC concentration, combined.

The data of LDSA exposure associated with BC concentration is at Figure 28. Moreover, by using an available data, $PCC = 0.04$. Next figure, considering PM1 and BC concentration values (Figure 30).

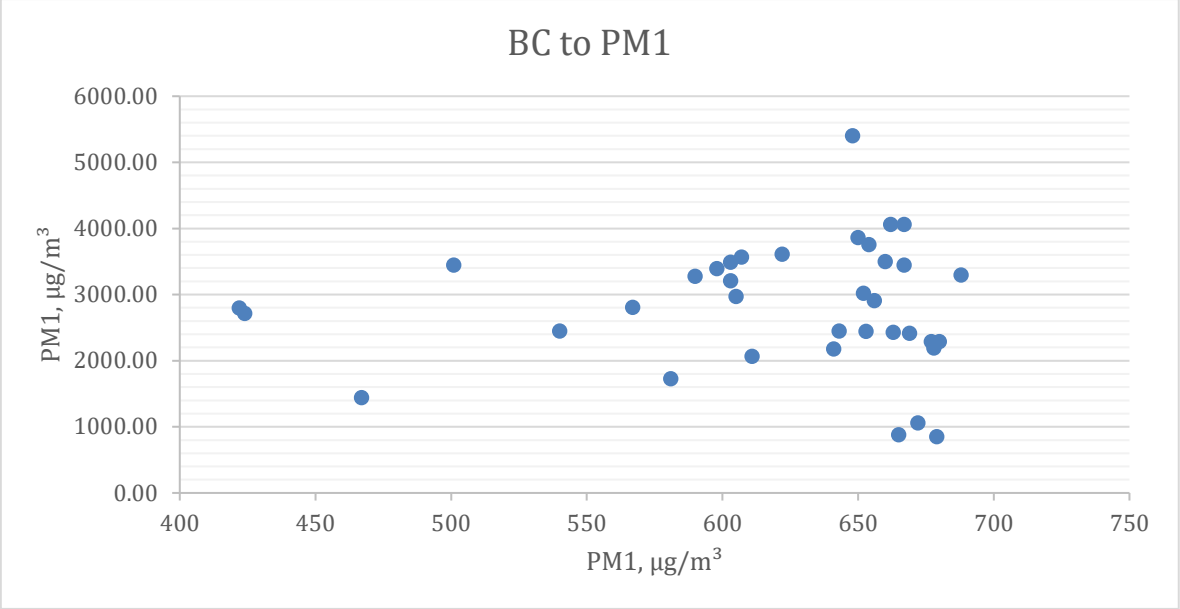

Figure 30. PM1 to BC concentration, combined.

The analysis of measurements done using four tools. The results of all Days of measurements showed that growth of air velocity lead to decrease of exposure of LDSA, black carbon and PM1 concentrations, since the Pearson correlation coefficients shows negative correlations, in some cases, the correlation is almost zero. Thus, for Day 1 the air velocity to PM1 is $PCC = -0.07$, as well as for LDSA is $PCC = -0.27$. From the Day 2, the air velocity associate with black carbon concentration $PCC = -0.01$; LDSA exposure $PCC = -0.15$; and from PM1 $PCC = -0.07$. From the Day 3 results, the air velocity $PCC = -0.4$ for both, black carbon concentration and LDSA exposure.

This analysis will help to use the relations of PM1 and BC in estimations of DPM emissions. As diesel engines produces around 45-88% of PM1 and BC is also indicating of exposure to diesel exhaust. In the combustion process, elemental carbon (EC) emissions are part of the DPM (about 80%). Total carbon (TC) is represented at 80 percent in DPM, which is similar to the representation of elemental carbon. Thus, RizgardPM and Microaeth instrumentations can suitable tools for monitoring DPM emissions.

4.3 Data Preparation for Modeling

According to the results obtained and analyzed correlation trends, Figure 31a presents air velocity data for 9 points for distance from 5.5m from LHD. In addition to that, Figure 31b represents corresponding PM1 values.

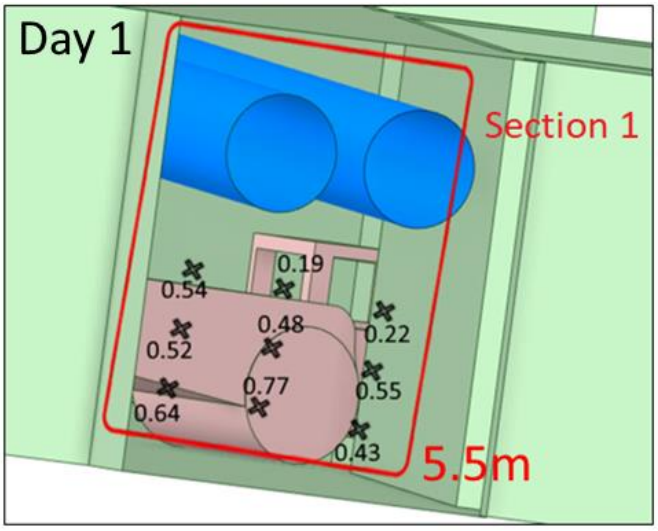

a) air velocity for Day 1, section 1.

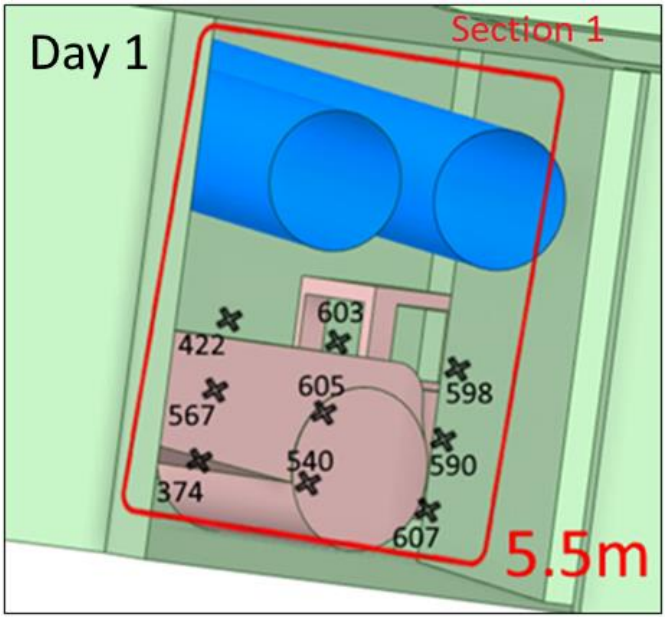

b) PM1 concentrations for Day 1, Section 1.

Figure 31. a) Velocity measurements in m/s; b) PM1 measurements in µg/m³.

In addition to that, the results of velocity, as well as PM1 are presented at Figure 32a and Figure 32b from 14.45m distance from LHD measurements.

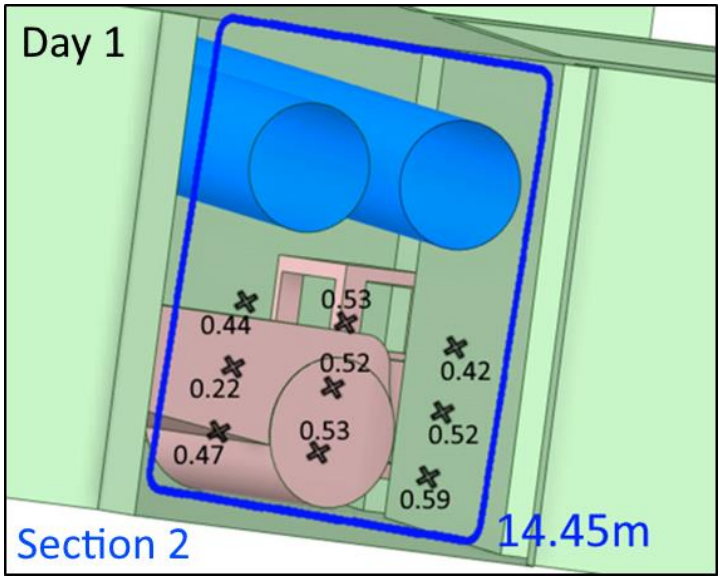

a. Results of velocity measurements from 14.45m, in m/s.

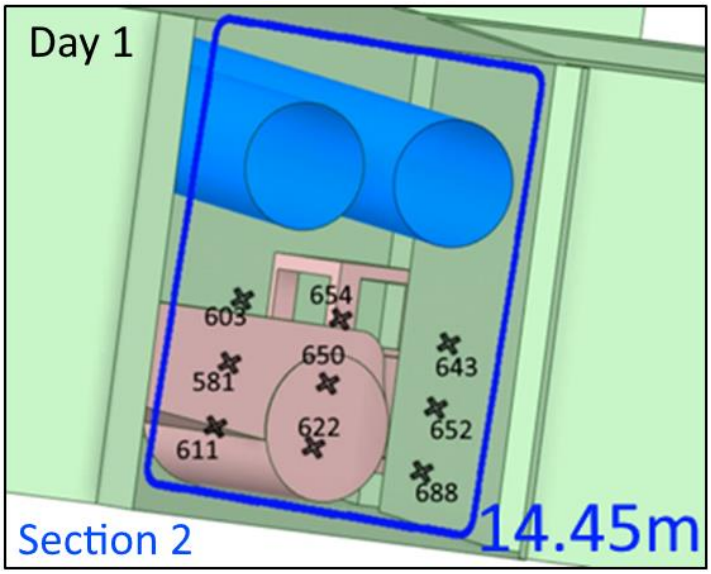

b. Results of PM1 measurements from 14.45m, in μg/m³.

Figure 32 a, b. Results of velocity and PM1 measurements from 14.45m, in m/s and μg/m³, (section 2).

PM1 concentrations are detected in places with low air velocity, as shown in Figure 31 and Figure 32 (cross cut). Additionally, the PM1 levels are greater in the LHD exhaust projection. The highest values of PM1 concentrations are seen from the right side of the wall. That may be due to location of exhaust pipe that installed on the projection of the ride side of the wall.

Additional representation of the measured results is at Figure 33a and Figure 33b. Figure 33a shows data of velocity for 5.6m and 4.7m meters, which are exhaust air, and inlet air (drift). From the Day 3 data, the velocity profile is presented at Figure 33b.

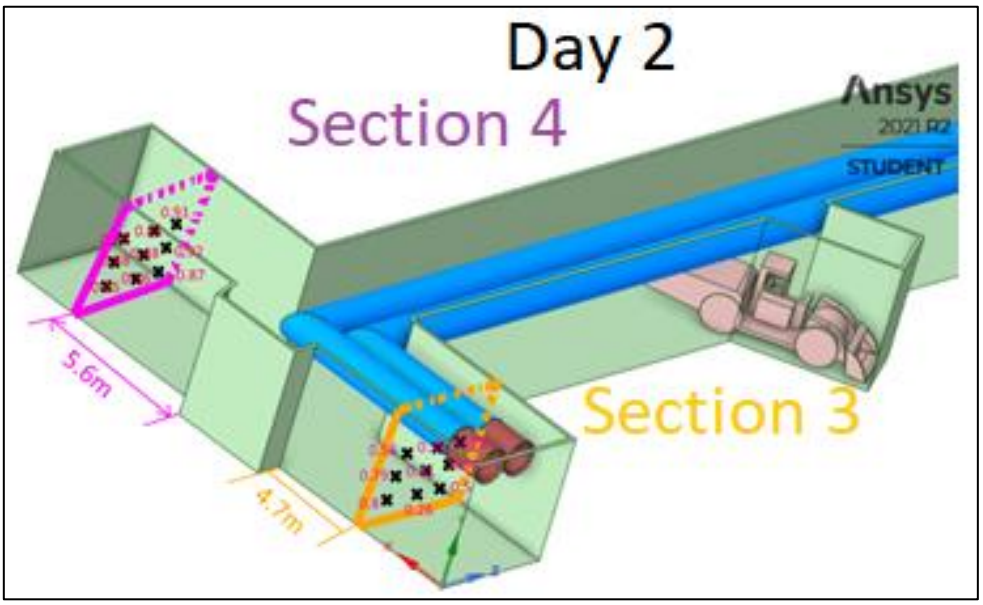

a. Results of velocity measurements from 5.6m and 4.7m, in m/s.

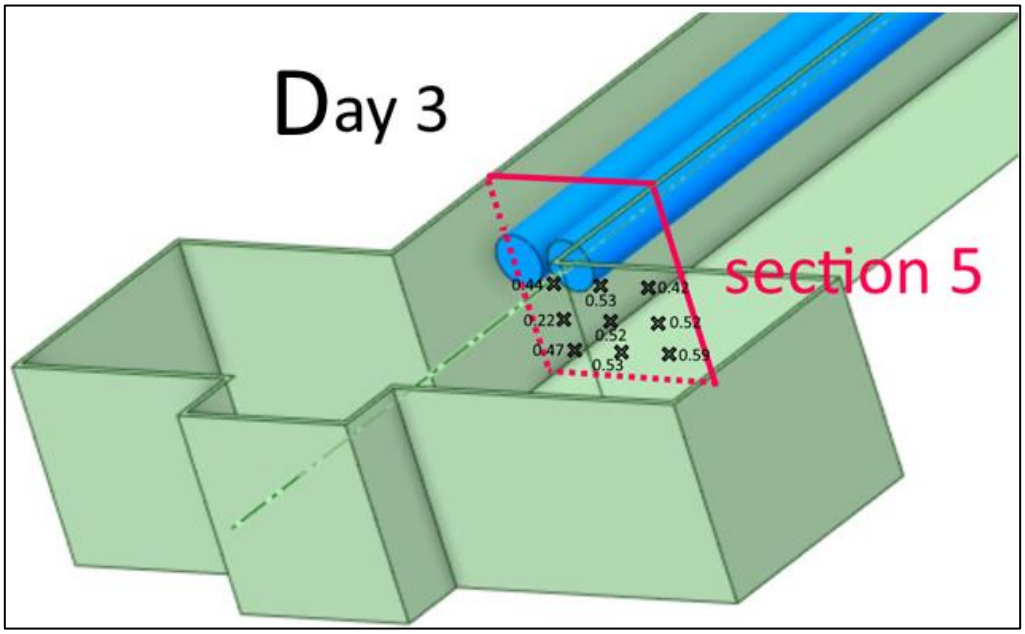

b. Results of velocity measurements from 2 m, in m/s.

Figure 33. Results of velocity measurements from Section 3, Section 4, and Section 5

These three days measurements data can be used to validate ventilation simulation model. The preliminary results of air velocity simulation is done for 5.5m and 14.45m.

4.4 CFD Modelling

The main expectation from simulation is to receive data same to real measurements. As a result, strategies can be developed to control pollutants in diesel fuel. After setting boundary conditions, mathematical models, and solution methods from methodology, the velocity profile has been achieved at ANSYS software (Figure 34).

Boundary conditions for air velocity concentration:

- Velocity inlet for LHD exhaust pipe is 47.8 m/s;
- Total temperature: 24℃;
- Velocity inlet for each auxiliary duct is 17.0 m/s.

Total temperature set as an average value from the measured results after anemometer data. The “inlets” were set as from velocity from exhaust pipe, and for each auxiliary duct. The velocity from auxiliary duct is calculated from manufacturer (Type ESN 9-450), by using the duct’s diameter and available volumetric airflow. As results Figure 34 presents air velocity profile for the active ore heading area. Most velocities are in a range of 0.7-1.2 m/s that is correspond to the measured velocities. The location of the LHD is static and not moving.

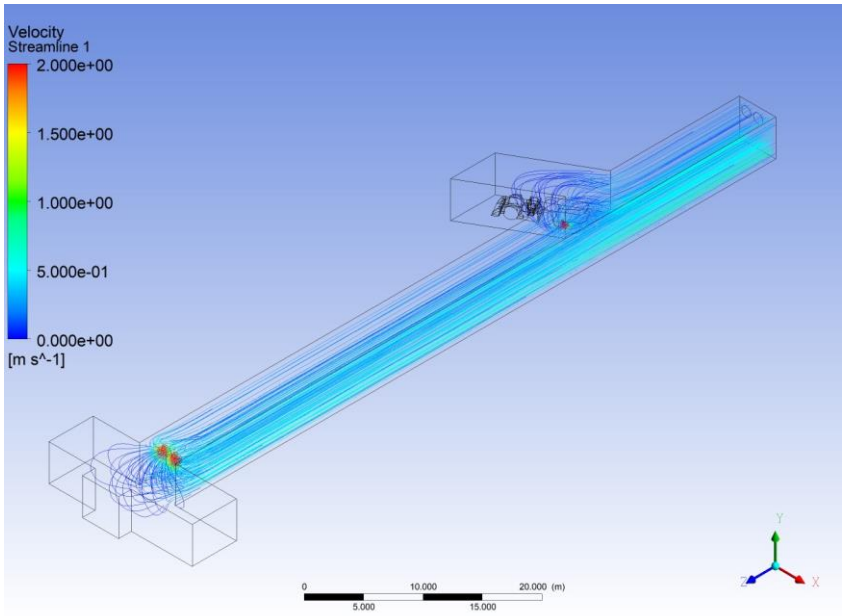

Figure 34. Velocity profile.

For simulation, the loader assumed not moving, but with working engine, and was located in the loading chamber (Figure 34). In the figure 34, the red zones are those, where the

velocity is higher that 2 m/s. In particular, the zones after ducts and exhaust pipe of the LHD. These zones were included as boundary conditions. These boundary conditions are: auxiliary ducts are 17 m/s, and for LHD exhaust is 47.8 m/s. Considering the boundary conditions (temperature, auxiliary duct and exhaust pipe velocity), the Figure 35 below represents simulation results for the measured areas.

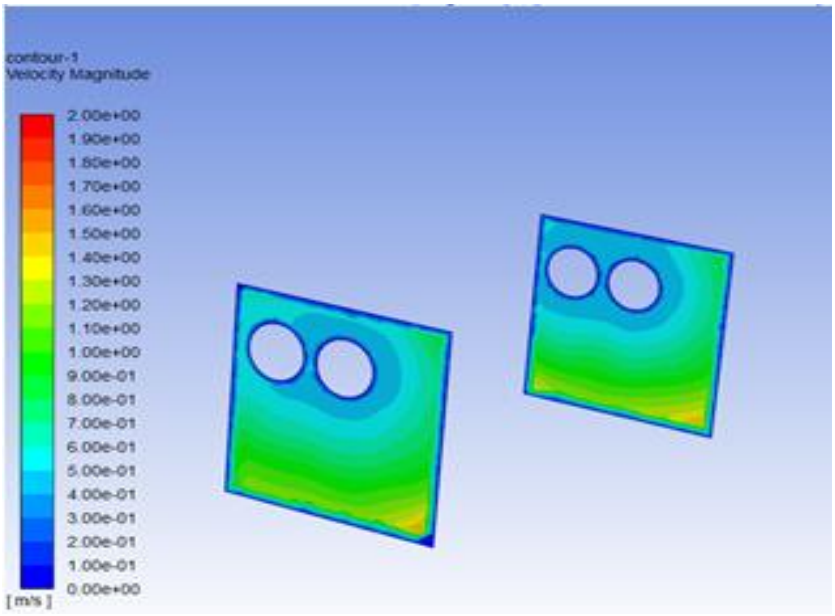

Figure 35. Air velocity profile for the measurement areas.

Considering the boundary conditions, the Figure 35 represents simulation results for the 5.5m and 14.45m measured areas. For the comparison purpose, the visual representation of measured 5.5m and 14.45m distance values is given at Figure 36.

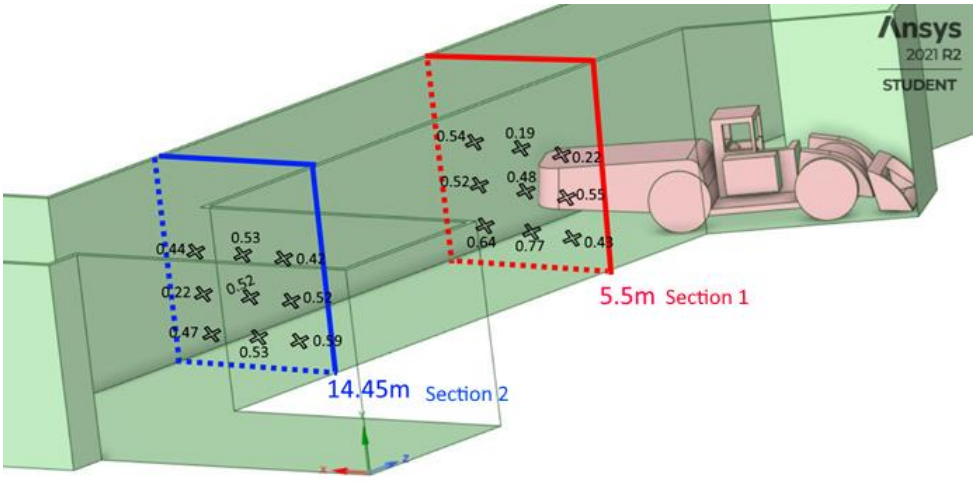

Figure 36. The measurements result.

According to the achieved results, the 9 points that are equal to those from where the measurements were done, contain simulated values (Figure 37). Also, this figure include time when the sampling of air velocity is done.

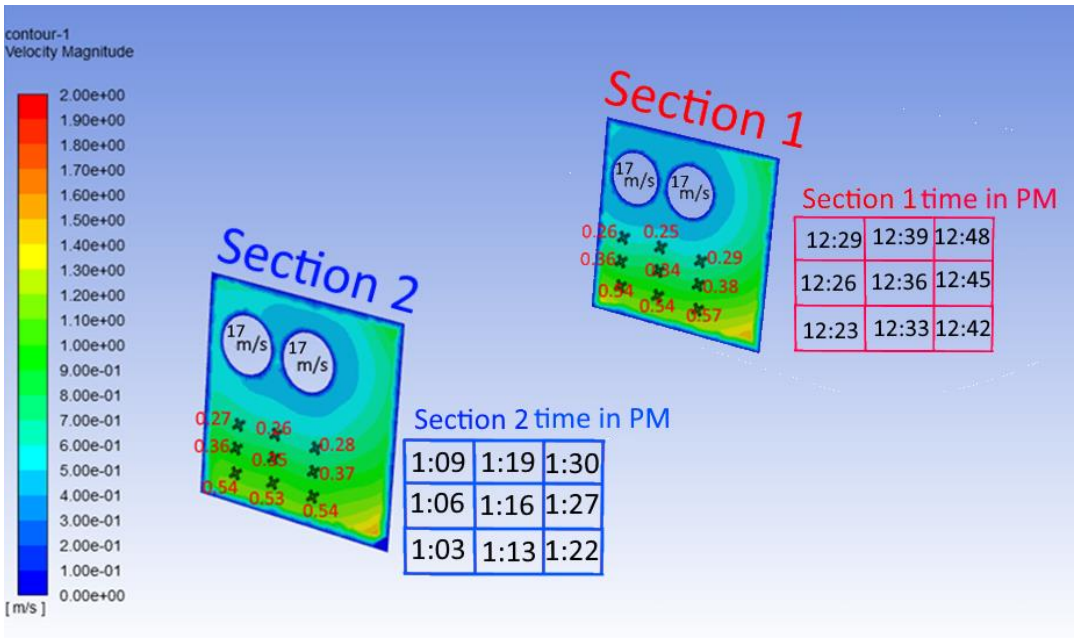

Figure 37. The velocity simulation results.

Figure 36 shows the velocity distribution among the cross-section from the simulation. From the received results after simulation, the difference between measured results at 9 points are 32% for 5.5m and 35% for 14.45m. These results are attached at Appendix 1 of this document.

5. DISCUSSION

The analysis of measurements done using four instrumentations: RizgardPM, Microaeth, Partector and anemometer. The results of all Days of measurements showed that growth of air velocity lead to decrease of exposure of LDSA, black carbon and PM1 concentrations, since the Pearson correlation coefficients shows negative correlations. The results of these correlation could be used for further analysis of different measuring tools.

The results of measuring tools used for preliminary air velocity simulation. However, this simulation doesn't consider position of the LHD loader. Thus, this has to be included to the boundary conditions for the specified case. Preliminary simulations have been produced (Figure 38) below. The Figure 38 consist the air velocity across the LHD loader. Due to restricted functions of the software student's version and time these simulations are recommended to be done for future work.

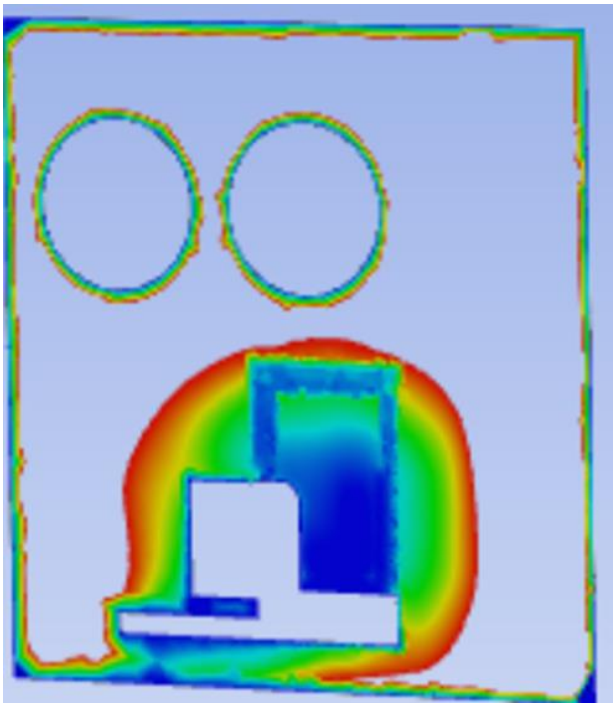

Figure 38. Preliminary simulation result.

For DPM simulation can be produced based on obtained relationships of air velocities and PM1 values. Moreover, BC and LDSA analyzed data are available to build other models. The LDSA values could be used as a baseline for measures, taken directly from the cabin of LHD.

6. CONCLUSIONS AND RECOMMENDATIONS

The main aim of this thesis was to conduct experimental measurements by various instrumentations to analyse data for modelling DPM concentrations in underground mines. A comprehensive literature review on DPM emissions measurements in underground mines, mine ventilation CFD modeling, DPM control strategies has been conducted. Based on the literature review, the analysis of dataset is proposed for this thesis. A methodology for experimental measurements was proposed and the experimental measurements in underground mine conditions have been conducted.

Received data from the experimental measurements conducted by various instrumentations: RizgardPM, Microaeth and Partector. PM1 concentration determined with RizgardPM for aerosol particles with sizes in PMs range. For 75 minutes of observation, PM1 average concentration of 620 $\mu g/m^3$ has been measured. LDSA readings from Naneos Partector 2 indicated average concentration of 4600 $\mu m^2/cm^3$. Microaeth showed an average BC concentration of 2900 $\mu g/m^3$. Moreover, during the measurements the average particle diameter is 100 nm, according to the Partector tool measurements. From the results, the correlation analysis between PM1, LDSA, BC data and air velocity data are done. These correlation results can be used for further research, as well as if data from one tool is not available.

Received data is valid to other measurements derived from the literature review and these findings suggest that using the RizgardPM and Microaeth to conduct continuous monitoring of DPM can be a practical implementation. PM1 has been correlated with BC and shows that BC = 2.9868 PM1 + 1284.2. Also, using data from RizgardPM tool, the estimation of total and elemental carbon could be done.

Analyzed data has been validated for CFD air velocities modelling of auxiliary ventilation in underground mines. From the received results after CFD simulation, the difference between measured and simulated air velocity results is 34%. It is recommended to produce further simulations considering position of the LHD loader and re-estimate the boundary conditions for the specified case. DPM simulation can be produced based on obtained relationships of air velocities and PM1 values. Moreover, BC and LDSA analyzed data are available to build other models. The LDSA values could be used as a baseline for measures, taken directly from the cabin of LHD. From a financial point of view, further research could highlight the optimization of the annual costs of auxiliary ventilation systems.

7. REFERENCES

ALNOR ROTATING VANE RVA501. (n.d.). *Anemometer*.

https://tsi.com/products/ventilation-test-instruments/alnor/alnor-rotating-vanes/alnor-rotating-vane-rva501/

Ansys fluent (2021). *Fluid Simulation Software.*

https://www.ansys.com/products/fluids/ansys-fluent

Aminossadati, S. M., & Hooman, K. (2008). Numerical simulation of ventilation air flow in underground mine workings. In *Proceedings of the 12th U.S./North American Mine Ventilation Symposium, Reno, NV*, pp. 253-259.

Barrett, C., Sarver, E., Cauda, E., Noll, J., Vanderslice, S., & Volkwein, J. (2019). Comparison of Several DPM Field Monitors for Use in Underground Mining Applications. In *Aerosol and Air Quality Research, 19(11),* 2367-2380.

Benesty, J., Chen, J., Huang, Y., & Cohen, I. (2009). Pearson Correlation Coefficient. *Springer Topics in Signal Processing, 1–4*. doi:10.1007/978-3-642-00296-0_5

Bennett, J. S., Crouch, K. G., & Shulman, S. A. (2003a). Control of wake-induced exposure using an interrupted oscillating jet. In *AIHA Journal, 64*(1), 24-29.

Bennett, J. S., Feigley, C. E., Khan, J., & Hosni, M. H. (2003b). Comparison of emission models with computational fluid dynamic simulation and a proposed improved model. In *AIHA Journal, 64*(6), 739-754.

Brake, R. (2013). Ventilation challenges facing the metalliferous sector. In *The Australian mine ventilation conference, Australia, Adelaide, South Australia: AUSIMM.*

Brown, D. M., Wilson, M. R., MacNee, W., Stone, V., & Donaldson, K. (2001). Size-dependent proinflammatory effects of ultrafine polystyrene particles: a role for surface area and oxidative stress in the enhanced activity of ultrafines. *Toxicology and applied pharmacology, 175(3),* 191-199.

Bugarski, A. D., Cauda, E. G., Janisko, S. J., Mischler, S. E., & Noll, J. D. (2011). Diesel

aerosols and gases in underground mines; guide to exposure assessment and control. Department of Health and Human Services, Public Health Service, Center for Disease Control and Prevention, *National Institute for Occupational Safety and Health,* Office of Mine Safety and Health Research.

Bugarski, A. D., Janisko, S. J., Cauda, E. G., Mischler, S. E., & Noll, J. D. (2012). *Controlling exposure to diesel emissions in underground mines.* SME.

CAT. R1700 LHD dimensions. https://www.cat.com/en_US/products/new/equipment/underground-hard-rock/underground-mining-load-haul-dump-lhd-loaders/730743084457382.html#

Chang, P., & Xu, G. (2019). Review of Diesel Particulate Matter Control Methods in Underground Mines. In *Proceedings of the 11th International Mine Ventilation Congress* (pp. 461-470). Springer, Singapore.

Chang, P., Xu, G., Zhou, F., Mullins, B., & Abishek, S. (2019). Comparison of underground mine DPM simulation using discrete phase and continuous phase models. *Process Safety and Environmental Protection, 127,* 45-55.

Choi, S., Park, J. H., Kim, W., Kim, S. W., Lee, K. H., Chung, T., ... & Park, D. U. (2020). Black Carbon Exposure Characteristics in Diesel Engine Vehicle-related Jobs. *Aerosol and Air Quality Research, 21,* 200675. https://doi.org/10.4209/aaqr.200675

Falk, L. K., Martin, V. S., & Keen, B. (2010). The role of computational fluid dynamics to reduce losses and increase airflow at Vale Inco's Coleman Mine. In *Proceedings of the 13th U.S./North American Mine Ventilation Symposium, Sudbury, Ontario, Canada*, pp. 415-423.

Gyamfi, S. (2020). Considerations and Development of a Ventilation on Demand System in Konsuln Mine. *Degree project, Luleå University of Technology.* https://www.diva-portal.org/smash/get/diva2:1472059/FULLTEXT01.pdf

Haney, R. A., Fields, K. G., & Vail, S. G. (1997). Evaluation of diesel particulate exposures and control technology in a nonmetal mine. In *Proceedings of the Sixth International Mine Ventilation Congress*, Pittsburgh, PA.

Heerden, J., & Sullivan, P. (1993). The application of CFD for evaluation of dust suppression and auxiliary ventilating systems. In *USA, CO, Littleton: Proceedings of the Sixth US Mine Ventilation Symposium* (pp. 479-484).

Hurtado, J. P., Gutiérrez, O., & Moraga, N. O. (2010). Numerical simulation of shock losses at the intake and exhaust raises of block caving production level drifts. In *Proceedings of the 13th U.S./North American Mine Ventilation Symposium, Sudbury, Ontario, Canada*, pp. 425-432

Jade, R. K., & Sastry, B. S. (2008). An experimental and numerical study of two-way splits and junctions in mine airways. In *12th US/North American Mine Ventilation Symposium* (pp. 293-298).

Janisko, S., & Noll, J. D. (2010). Field evaluation of diesel particulate matter using portable elemental carbon monitors. In *Proceedings of the 13th US/North American Mine Ventilation Symposium (pp. 47-52).* Sudbury, Ontario, Canada: MIRARCO-Mining Innovation.

Khan, M. U. (2017). Real-time diesel particulate matter monitoring in underground mine atmospheres, association with the standard method and related challenges. *Doctoral Dissertation, Missouri University of Science and Technology.* http://scholarsmine.mst.edu/doctoral_dissertations/2625/

Kimbal, K. C., Pahler, L., Larson, R., & VanDerslice, J. (2012). Monitoring diesel particulate matter and calculating diesel particulate densities using Grimm Model 1.109 real-time aerosol monitors in underground mines. In *Journal of occupational and environmental hygiene, 9(6),* 353-361.

Kreyling, W. G., Semmler, M., Erbe, F., Mayer, P., Takenaka, S., Schulz, H., ... & Ziesenis, A. (2002). Translocation of ultrafine insoluble iridium particles from lung epithelium to extrapulmonary organs is size dependent but very low. *Journal of Toxicology and Environmental Health, Part A, 65(20),* 1513-1530.

Levin, L. Y., & Semin, M. A. (2017). Conception of automated mine ventilation control system and its implementation on Belarussian potash mines. In *Proceedings of the 16th North American Mine Ventilation Symposium. –Colorado* (pp. 17-1).

Location of exhaust pipe of LHD R1700. https://youtu.be/sUujh8Fgrhg

McGinn, S. (2000). The relationship between diesel engine maintenance and exhaust emissions.

Microaeth (n.d.). *Ma200, Aethlabs.* https://aethlabs.com/microaeth/ma200/overview

Mischler, S. E., & Colinet, J. F. (2010). Controlling and monitoring diesel emissions in underground mines in the United States. In *Mine Ventilation: Proceedings of the Ninth International Mine Ventilation Congress, New Delhi, India, pp. 879–888*.

Morla, R., & Karekal, S. (2017). Diesel particulate matter investigations in underground coal mines. International Journal of Engineering and Technology, 9 (4) (2017), pp. 2698-2703, 10.21817/ijet/2017/v9i4/170904401

Nagelkerke, N. J. (1991). A note on a general definition of the coefficient of determination. *Biometrika*, *78*(3), 691-692.

Nieto, A., Schatz, R. S., & Dogruoz, C. (2020). Performance analysis of electric and diesel equipment for battery replacement of tethered LHD vehicles in underground mining. *Mining Technology*, *129(1),* 22-29.

Noll, J. D., Bugarski, A. D., Patts, L. D., Mischler, S. E., & McWilliams, L. (2007). Relationship between elemental carbon, total carbon, and diesel particulate matter in several underground metal/non-metal mines. *Environmental science & technology*, *41(3),* 710-716.

Noll, J., & Janisko, S. (2007). Using laser absorption techniques to monitor diesel particulate matter exposure in underground stone mines. In *Smart Biomedical and Physiological Sensor Technology V* (Vol. 6759, p. 67590P). International Society for Optics and Photonics.

Noll, J., & Janisko, S. (2013). Evaluation of a wearable monitor for measuring real-time diesel particulate matter concentrations in several underground mines. In *Journal of occupational and environmental hygiene, 10(12),* 716-722.

Oberdörster, G., Sharp, Z., Atudorei, V., Elder, A., Gelein, R., Kreyling, W., & Cox, C.

(2004). Translocation of inhaled ultrafine particles to the brain. *Inhalation toxicology, 16(6-7),* 437-445.

PARTECTOR 2. (n.d.). *The world's smallest multimeric nanoparticle detector*. https://www.naneos.ch/partector2.html

Purushotham, T., & Bandopadhyay, S. (2010). Analyzing shock losses at air-crossings in a mine ventilation network using CFD simulations. In *Proceedings of the 13th U.S./North American Mine Ventilation Symposium, Sudbury, Ontario, Canada,* pp. 463-468.

Ristovski, Z. D., Miljevic, B., Surawski, N. C., Morawska, L., Fong, K. M., Goh, F., & Yang, I. A. (2012). Respiratory health effects of diesel particulate matter. *Respirology, 17*(2), 201-212.

RizgardPM (n.d.). *Plus. RizgardPM, PM monitor.* http://rizgardpa.com/#promotion

Robinson, M. A., Olson, M. R., Liu, Z. G., & Schauer, J. J. (2015). The effects of emission control strategies on light-absorbing carbon emissions from a modern heavy-duty diesel engine. Journal of the Air & Waste Management Association, 65(6), 759-766.

Saarikoski, S., Salo, L., Bloss, M., Alanen, J., Teinilä, K., Reyes, F., ... & Timonen, H. (2019). Sources and Characteristics of Particulate Matter at Five Locations in an Underground Mine. *Aerosol and Air Quality Research, 19(12),* 2613-2624.

Sagesh Kumar, M. R., Dash, A. K., Bhattcharjee, R. M., & Panigrahi, D. C. (2018). Diesel Exhaust and Diesel Particulate Matter (DPM) in Underground M of India. *Proceedings of the 11th International Mine Ventilation Congress,* 483–492. Doi: 10.1007/978-981-13-1420-9_41

Srinivasa, R.B., Baafi, E.Y., Aziz, N.I. and Singh, R.N. (1993) Three dimensional numerical modelling of air velocities and dust control techniques in a longwall face. In *Proceedings of the Sixth U.S. Mine Ventilation Symposium,* Salt Lake City, UT, pp. 287–292.

Stanek, L. W., & Brown, J. S. (2019). Air Pollution: Sources, Regulation, and Health Effects. In *Reference Module in Biomedical Sciences, Elsevier*, pp. 1–10.

Stephens, M., & Calizaya, F. (2010). A study of leakage flow in a laboratory model and using CFD. In *Proceedings of the 13th U.S./North American Mine Ventilation Symposium, Sudbury, Ontario, Canada,* pp. 485-491.

Stephenson, D. J., Lutte, M. G., & Spear, T. M. (2006). Evaluation of Sampling Methods to Measure Exposure to Diesel Particulate Matter in An Underground Metal Mine. In *1st Annual Regional National Occupational Research Agenda (NORA) Young/New Investigators Symposium.*

Thiruvengadam, M., Zheng, Y., & Tien, J. C. (2016). DPM simulation in an underground entry: Comparison between particle and species models. *International Journal of Mining Science and Technology, 26(3),* 487-494.

Torano, J., Torno, S., Menéndez, M., & Gent, M. (2011). Auxiliary ventilation in mining roadways driven with roadheaders: Validated CFD modelling of dust behavior. *Tunneling and Underground Space Technology, 26(1), 201–210.* doi:10.1016/j.tust.2010.07.005

Type ESN 9-450. (n.d.) *Axial Flow Fan, CST.* https://cst-germany.com/en/product/axial-flow-fan-type-esn-9-450-id166

Type ESN 9-450. (n.d.) *SNKS Machine sales. Technical specifications.* https://snskmachinesales.com/wp-content/uploads/2019/04/Kormann-ES-3.pdf

VentSim Lite (2018). *Integrated mine and tunnel ventilation software package.* *https://ventsim.com/ventsim-lite/*

Wala, A. M., Yingling, J. C., Zhang, J., & Ray, R. (1997). Validation study of computational fluid dynamics as a tool for mine ventilation design. *In Proceedings of the 6th international mining ventilation congress, Pittsburgh.*

Wala, M.A., Jacob, Huang, P.G., and Brown, J.T. (2003). A new approach to evaluate mine face ventilation. In *Mining Engineering, Vol. 55 (No. 3),* pp. 25-30.

Wala, A. M., Vytla, S., Taylor, C. D., & Huang, G. (2007). Mine face ventilation: a comparison of CFD results against benchmark experiments for the CFD code validation. In *Mine Engineering, Vol. 59 (No. 10),* pp. 49-55.

Wala, A. M., Vytla, S., Huang, G., & Taylor, C. D. (2008). Study on the effects of scrubber operation on the face ventilation. In *Proceedings of the 12th US/North American Mine Ventilation Symposium* (Vol. 12, pp. 281-286).

Yang, S., Deng, C., Gao, Y., & He, Y. (2016). Diesel particulate filter design simulation: A review. *Advances in Mechanical Engineering*, *8(3).*

Zheng, Y. (2011). Diesel particulate matter dispersion analysis in underground metal/non-metal mines using CFD. *Missouri university of science and technology, Ph. D. thesis.*

Zheng, Y., Thiruvengadam, M., Lan, H., & Tien, J. (2015). Simulation of DPM distribution in a long single entry with buoyancy effect. International Journal of Mining Science and Technology, 25(1), 47-52.

Zheng, Y., & Tien, J. C. (2009). Simulation of methane distribution at longwall face. In *2009 SME Annual Meeting. Denver* (pp. 1-8).

APPENDIX 1

point (5.5)	measurement [m/s]	sim [m/s] (2)	%error	sim [m/s] (3.5)	%error	sim [m/s] (2.8)	%error	sim [m/s] (2.9)	%error	sim [m/s] (3.1)	%error
1	0,64	0,39	39,80	0,60	5,97	0,50	21,14	0,52	18,77	0,55	13,88
2	0,77	0,39	49,98	0,60	21,78	0,50	34,42	0,52	32,45	0,55	28,37
3	0,43	0,41	4,26	0,64	-49,00	0,54	-25,51	0,56	-29,28	0,59	-37,09
4	0,52	0,26	49,98	0,41	20,89	0,34	34,45	0,35	32,53	0,37	28,49
5	0,48	0,25	48,30	0,40	16,30	0,33	32,28	0,33	30,29	0,35	26,12
6	0,55	0,27	50,33	0,44	20,28	0,36	34,96	0,37	33,04	0,39	29,03
7	0,54	0,19	65,50	0,31	43,26	0,24	54,77	0,25	53,45	0,27	50,69
8	0,19	0,18	4,81	0,30	-59,75	0,24	-24,86	0,24	-28,47	0,26	-36,01
9	0,22	0,21	6,77	0,34	-53,75	0,27	-22,24	0,28	-25,80	0,29	-33,30
			41,93		37,05		33,08		32,77		32,80

point (14.45)	measurement [m/s]	sim [m/s] (2)	%error	sim [m/s] (3.5)		sim [m/s] (2.8)	%error	sim [m/s] (2.9)	%error	sim [m/s] (3.1)	%error
1	0,47	0,39	16,97	0,60	-28,47	0,51	-8,46	0,53	-11,82	0,56	-18,37
2	0,53	0,38	28,72	0,59	-11,68	0,50	6,56	0,51	3,65	0,54	-2,05
3	0,59	0,39	33,79	0,62	-4,71	0,51	12,97	0,53	10,26	0,56	4,90
4	0,22	0,26	-18,29	0,41	-88,45	0,34	-54,54	0,35	-59,39	0,37	-68,71
5	0,52	0,25	52,16	0,40	22,47	0,33	37,29	0,34	35,32	0,36	31,50
6	0,52	0,26	49,07	0,43	17,32	0,35	33,08	0,36	30,97	0,38	26,86
7	0,44	0,20	55,23	0,32	27,03	0,26	41,44	0,27	39,61	0,28	36,07
8	0,53	0,19	65,03	0,31	41,36	0,24	54,11	0,25	52,66	0,27	49,88
9	0,42	0,20	52,13	0,33	20,31	0,26	36,97	0,27	34,96	0,29	31,08
			44,37		37,20		36,14		35,83		35,83